



**International Journal  
of Engineering &  
Applied Sciences**

I  
J  
E  
A  
S

IJEAS

Volume 16, Issue 4  
2024

## **HONORARY EDITORS**

*(in alphabetical order)*

Prof. Atluri, S.N.- University of California, Irvine-USA  
Prof. Liew, K.M.- City University of Hong Kong-HONG KONG  
Prof. Lim, C.W.- City University of Hong Kong-HONG KONG  
Prof. Liu, G.R.- National University of Singapore- SINGAPORE  
Prof. Nath, Y.- Indian Institute of Technology, INDIA  
Prof. Omurtag, M.H. -ITU  
Prof. Reddy, J.N.-Texas A& M University, USA  
Prof. Saka, M.P.- University of Bahrain-BAHRAIN  
Prof. Shen, H.S.- Shanghai Jiao Tong University, CHINA  
Prof. Xiang, Y.- University of Western Sydney-AUSTRALIA  
Prof. Wang, C.M.- National University of Singapore- SINGAPORE  
Prof. Wei, G.W.- Michigan State University-USA

## **EDITOR IN CHIEF:**

Assoc. Prof. Ibrahim AYDOĞDU -Akdeniz University [aydogdu@akdeniz.edu.tr](mailto:aydogdu@akdeniz.edu.tr)

## **ASSOCIATE EDITOR:**

Assist. Prof. Kadir MERCAN –Mehmet Akif Ersoy  
University [kmercan@mehmetakif.edu.tr](mailto:kmercan@mehmetakif.edu.tr)

## **SECTION EDITORS:**

Assoc. Prof. Metin Mutlu Aydın – Ondokuz Mayıs University  
Assoc. Prof. Mustafa Arda –Trakya University  
Assist. Prof. Refik Burak Taymuş- Van 100. Yıl University  
Dr. Shahin Nayyeri Amiri- Old Dominion University

### **LANGUAGE EDITOR:**

Instructor Gülseren Aslı Seçmen– Akdeniz University

### **LAYOUT EDITOR:**

Dr. Instructor Seda Turan– Antalya Belek University

### **EDITORIAL BOARD**

*(The name listed below is not Alphabetical or any title scale)*

Prof. Xinwei Wang -Nanjing University of Aeronautics and Astronautics

Asst. Prof. Francesco Tornabene -University of Bologna

Asst. Prof. Nicholas Fantuzzi -University of Bologna

Assoc. Prof. Keivan Kiani - K.N. Toosi University of Technology

Asst. Prof. Michele Baccocchi -University of Bologna

Asst. Prof. Hamid M. Sedighi -Shahid Chamran University of Ahvaz

Prof. Yaghoub Tadi Beni -Shahrekord University

Prof. Raffaele Barretta -University of Naples Federico II

Prof. Meltem ASİLTÜRK -Akdeniz University *meltemasilturk@akdeniz.edu.tr*

Prof. Metin AYDOĞDU -Trakya University *metina@trakya.edu.tr*

Prof. Ayşe DALOĞLU - KTU *aysed@ktu.edu.tr*

Prof. Oğuzhan HASANÇEBİ - METU *oguzhan@metu.edu.tr*

Asst. Prof. Rana MUKHERJİ - The ICFAI University

Assoc. Prof. Baki ÖZTÜRK - Hacettepe University

Assoc. Prof. Yılmaz AKSU -Akdeniz University

Assoc. Prof. Hakan ERSOY- Akdeniz University

Assoc. Prof. Mustafa Özgür YAYLI -Uludağ University

Assoc. Prof. Selim L. SANİN - Hacettepe University

Asst. Prof. Engin EMSEN -Akdeniz University

Prof. Serkan DAĞ - METU

Prof. Ekrem TÜFEKÇİ - İTÜ

## ABSTRACTING & INDEXING



IJEAS provides unique DOI link to every paper published.

## EDITORIAL SCOPE

The journal presents its readers with broad coverage across some branches of engineering and science of the latest development and application of new solution algorithms, artificial intelligent techniques innovative numerical methods and/or solution techniques directed at the utilization of computational methods in solid and nano-scaled mechanics.

International Journal of Engineering & Applied Sciences (IJEAS) is an Open Access Journal

International Journal of Engineering & Applied Sciences (IJEAS) publish original contributions on the following topics:

**Civil Engineering:** numerical modelling of structures, seismic evaluation, experimental testing, construction and management, geotechnical engineering, water resources management, groundwater modelling, coastal zone modelling, offshore structures, water processes, desalination, waste-water treatment, pavement and maintenance, transport and traffic, laser scanning, and hydrographic surveying, numerical methods in solid mechanics, nanomechanic and applications, microelectromechanical systems (MEMS), vibration problems in engineering, higher order elasticity (strain gradient, couple stress, surface elasticity, nonlocal elasticity)

**Electrical Engineering:** artificial and machine intelligence and robotics, automatic control, bioinformatics and biomedical engineering, communications, computer engineering and networks, systems security and data encryption, electric power engineering and drives, embedded systems, Internet of Things (IoT), microwaves and optics.

**Engineering Mathematics and Physics:** computational and stochastic methods, optimization, nonlinear dynamics, modelling and simulation, computer science, solid state physics and electronics, computational electromagnetics, biophysics, atomic and molecular physics, thermodynamics, geophysical fluid dynamics, wave mechanics, and solid mechanics.

**Mechanical Engineering:** machine design, materials science, mechanics of materials, manufacturing engineering and technology, dynamics, robotics, control, industrial engineering, ergonomics, energy, combustion, heat transfer, fluids mechanics, thermodynamics, turbo machinery, aerospace research, aerodynamics, and propulsion.

IJEAS allows readers to read, download, copy, distribute, print, search, or link to the full texts of articles.





# CONTENTS

## **Stake - Out of Curves with the Polar Method: Application in Trumpet Type Intersections**

*By Mehmet EREN, Aziz Uğur TONA ..... 165-178*

## **Investigating Solar Energy Potential in Afghanistan under Certain Climatic and Geometrical Parameters of Cities and Buildings**

*By Edris NASERİ , Burcin Deda ALTAN, Afşin GÜNGÖR..... 179-194*

## **Assessment of Concrete Pavement Performance on Istanbul's BRT Lines**

*By Aydın KICI..... 195-206*

## **Finite Element Analysis of Concrete Gravity Dam**

*By Tuba AYDIN ..... 207-218*

## Stake - Out of Curves with the Polar Method: Application in Trumpet Type Intersections

Mehmet Eren <sup>1</sup>, Aziz Uğur Tona <sup>2\*</sup>

<sup>1</sup> Yıldız Teknik Üniversitesi, İnşaat Fakültesi, Harita Mühendisliği Bölümü, İstanbul, Türkiye

<sup>2</sup> Gümüşhane Üniversitesi, Mühendislik ve Doğa Bilimleri Fakültesi, Harita Mühendisliği Bölümü, Gümüşhane, Türkiye

✉: [meren@yildiz.edu.tr](mailto:meren@yildiz.edu.tr) <sup>1</sup> , [azizugurtona@gumushane.edu.tr](mailto:azizugurtona@gumushane.edu.tr) <sup>2\*</sup> : 0000-0002-8370-8615 <sup>1</sup>, 0000-0001-7367-7731 <sup>2\*</sup>

Received: 04.10.2024, Revised: 21.10.2024, Accepted: 11.11.2024

### Abstract

*The sustainability and efficiency of modern infrastructure are directly related to effective highway design. The increasing demands of industrialization, tourism, and trade have highlighted the need for fast and safe transportation. Trumpet-type interchanges provide a significant solution for these transportation needs. This study examines how the intermediate points of curves used in the connecting roads of trumpet-type interchanges can be staked out using the polar method. The research provides a detailed explanation of how to determine intermediate points of curve elements both at project and land level, supported by simulated data. The results offer a practical approach to enhancing accuracy and efficiency in engineering projects.*

**Keywords:** Interchange with different levels, inverted curve, Curve stake out with polar method, Trumpet type intersection

### 1. Introduction

Industrialization, tourism activities, and the marketing of commercial products domestically and internationally have increased the mobility of highways today. Bridged interchanges and connecting routes are designed for quick transportation between cities and nearby areas. The connection paths can be in various forms; they may be in the form of a trumpet or in the form of two successive inverse curves (Figs. 1-4) [1-3]. There is usually a certain level of difference in the trumpet-shaped connection path between the entrance and exit points of the main highways. The shape of the connecting highway on the outside of the trumpet interchange is in the form of an inverted curve in general appearance. The shape of the connecting path in the interior is a circular arc with a divergence angle greater than 200 grad (Figs. 1-2).

The general stake-out of curves in engineering is widely found in the literature [3-9]. Stake-out is one of the most crucial tasks for a surveying engineer since it allows them to meet the project's required accuracy standards while preserving the engineering structure's planned geometries [10-15]. Inverse curves are often used on urban and mountain roads where there is no high-speed limit. They are also used for longitudinal and transverse scrolling of a road leading to a line in highway projects from a certain point to a desired amount [5, 7]. Total stations are used to conduct construction surveys and layouts, even though modern GNSS systems have the potential to stake out points with an accuracy of 2 cm under better conditions. The polar coordinates approach, which involves calculating and estimating the position of a horizontal angle and a distance from two control points (or geodetic points), forms the basis of a total station stake-out [10].



Fig. 1. Trumpet interchange and connecting highways [16]

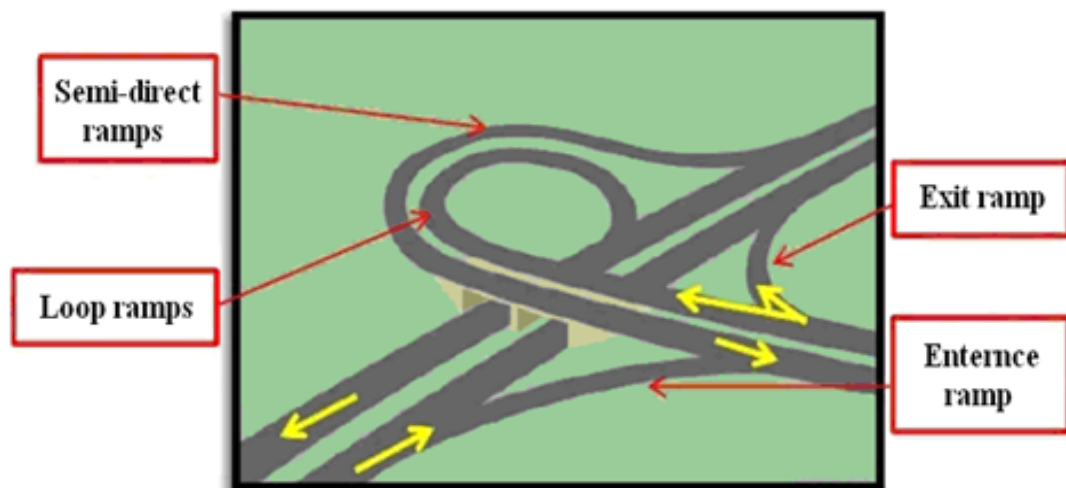


Fig. 2. Graphic illustration of trumpet interchange



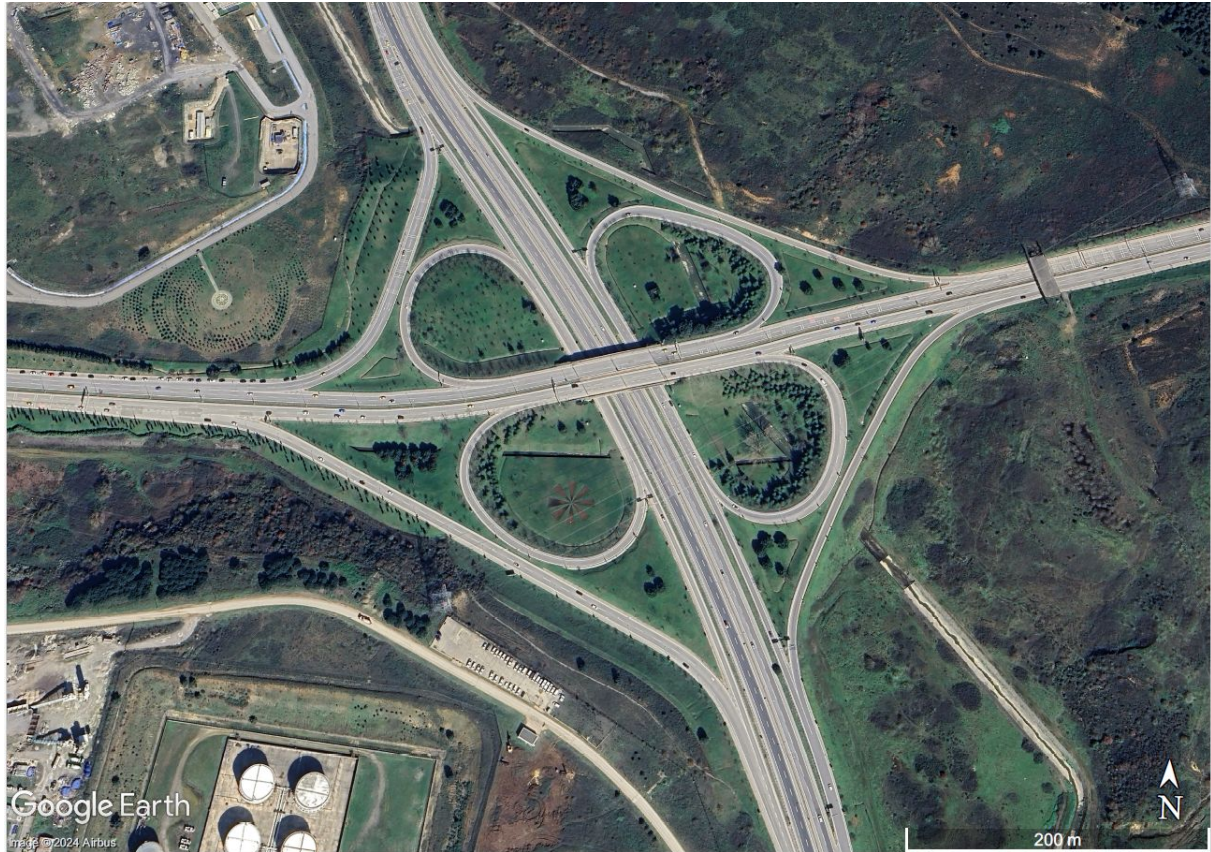


Fig. 3. The Cloverleaf interchange [16]

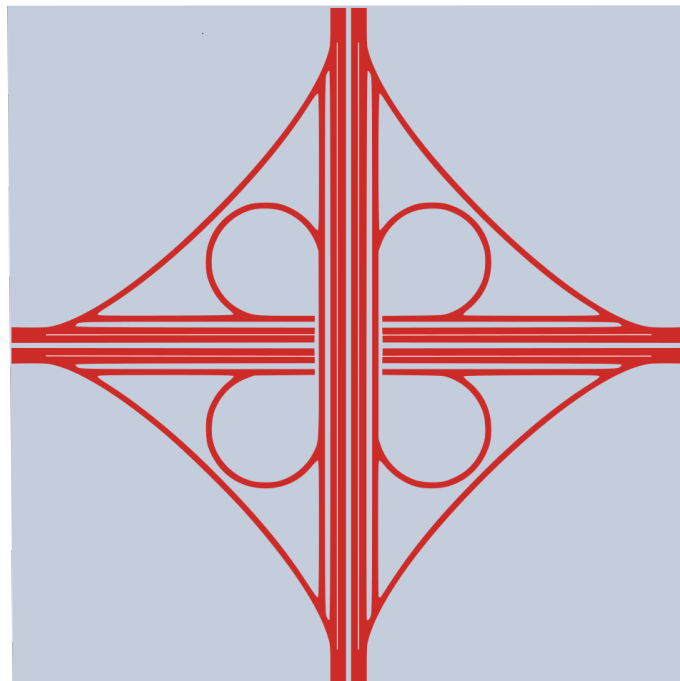


Fig. 4. Graphic illustration of the cloverleaf interchange

Inverse curve that forms the outer part of a trumpet interchange and the circular arc forming the inner part from points where curves are tangential to the main path how the inverse curve that forms the outer part of a trumpet interchange and the circular arc forming the inner part from

points where curves are tangential to the main path can be applied by the polar method was deemed necessary to investigate the matter as it was not explained in detail in the literature [3-9]. This study explains in detail the stake-out process for connection and tangential points of inner and outer connection paths to the upper and lower main highways at both land and project levels. It also covers the stake-out of intermediate points of related curves from tangent points at these levels. The numerical stake-out was applied, and the results are presented within the study [17]. Thus, it has contributed to filling the gap in the literature regarding the stake-out of trumpet type intersections.

## 2. Overview of the Trumpet Interchange

### 2.1. Stake-out of Top and Bottom Tilting Points of Inner and Outer Connection Highways at Trumpet Interchange

On a highway plan with a trumpet interchange (Fig. 5), the inner link path is between points A, B, G, E, and B' between circular arcs of radius  $R_1$  and  $R_2$  with center  $O_1$ , and the external link path is located between points C, E', F, H, E, and B' between the circle springs  $R_2$  and  $R_3$  with center  $O_1$  and circle springs  $R_4$  and  $R_5$  with center  $O_2$ . The deviation angle seen from the center of the inner connecting path is  $1 > 200$ , and the divergence angles of the inverse curve forming the external connection path are  $\Delta_2$  and  $\Delta_3$ .

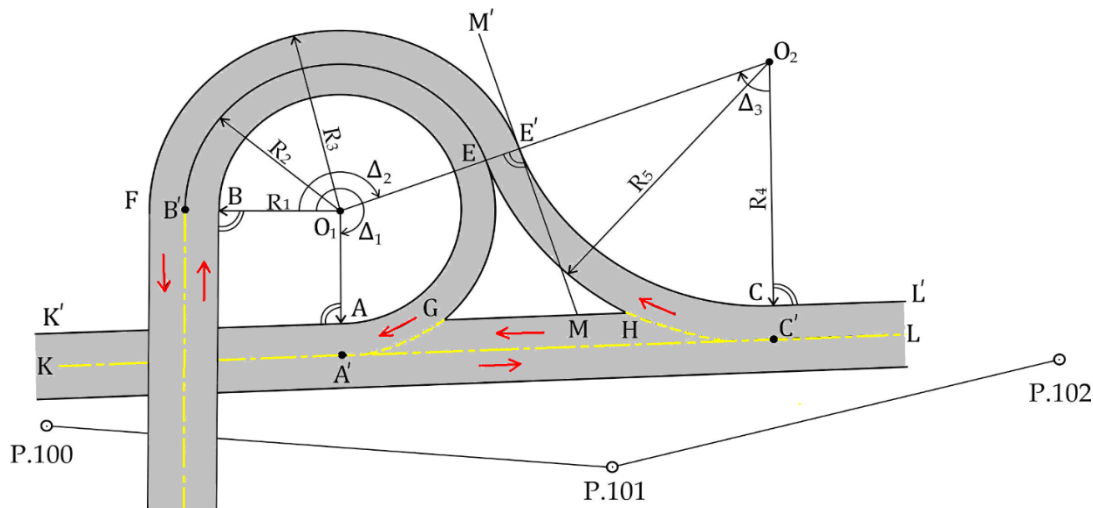


Fig. 5. At the trumpet interchange, the inner curve provides the reverse curve, and the inner connection forms the outer connection path.

In Fig. 5, point A is the point where the inner radius of the radius  $R_1$  is tangential to the right side of the subway platform. Point A' is the point at which the circular extension of the radially inner connection path  $R_2$  is tangential to the main axis (line KL).

- B point: the point  $O_1$  is tangent to the left side of the upper main highway platform of the radiused circle arc of radius  $R_1$ .
- Point B' is the point where  $O_1$  center  $R_2$  is radially tangent to the outer major axis of the outer and inner link paths.

- Point C is the point where the  $O_2$  center external link path  $R_4$  is tangent to the right side ( $K'L'$  line) of the lower highway platform.
- Point  $C'$  is the point at which the circular extension of the outer radius of the radius connection  $R_5$  is tangential to the axis of the subway (line  $KL$ ).
- Point  $E'$  is the point at which the outer radius of radius  $R_5$  is tangential to the inner radius of radius  $R_2$ .
- Point  $E$  is the point at which  $R_4$  is tangent to the radius of the outer connecting path and  $R_2$  is tangent to the radius of the inner connecting path.
- Point  $F$  is the point where the arc of radius  $R_3$  is tangent to the right side of the upper highway platform.
- Point  $G$  is the point of intersection on the right-hand side of the lower highway platform of the radiused circle arc.
- Point  $H$  is the intersection point of the right-hand side of the lower highway platform of the circle with  $R_5$ .
- Point  $M$  intersects the tangential  $GH$  line segment passing through the common tangent point  $R_3$  with  $O_1$  center  $R_3$  and  $O_2$  center  $R_4$  radiused edges  $E'$ .

In a highway plan (Fig. 5) where the trumpet interchange is located, these points ( $A, A', B, B', C, C', E, E', F, G, H, O_1, O_2, K, L$ ) are digitized and their coordinates are obtained.

The polar Stake-out components are calculated using the coordinates of the points where taking advantage of the two polygons ( $P.100, P.101$ ) previously set up around the Trumpet interchange and the coordinates of the specified points ( $\beta_A, \beta_{A'}, \beta_B, \beta_{B'}, \beta_C, \beta_{C'}, \beta_E, \beta_{E'}, \beta_F, \beta_G, \beta_H, \beta_K, \beta_{K'}, \beta_L, \beta_{L'}, P_{101}A, P_{101}A', P_{101}B, P_{101}B', P_{101}C, P_{101}C', P_{101}E, P_{101}E', P_{101}F, P_{101}G, P_{101}H, P_{101}K, P_{101}K', P_{101}L, P_{101}L'$ ). For example, stake-out elements for points  $A, B$  and  $C$  are calculated with the help of the following equations [6], (Fig. 6):

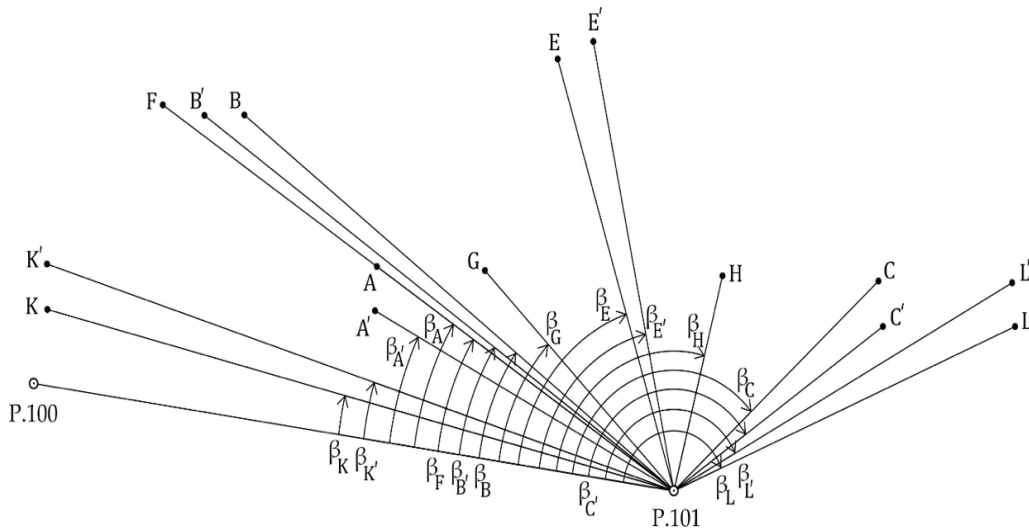


Fig. 6. Stake-out by using the polar method of fundamental points of trumpet interchange from P.101 point to P.100 point



$$P_{101}A = \sqrt{(Y_A - Y_{101})^2 + (X_A - X_{101})^2} \quad (1)$$

$$P_{101}B = \sqrt{(Y_B - Y_{101})^2 + (X_B - X_{101})^2} \quad (2)$$

$$P_{101}C = \sqrt{(Y_C - Y_{101})^2 + (X_C - X_{101})^2} \quad (3)$$

$$(P_{101}P_{100}) = \arctan\left(\frac{Y_{100} - Y_{101}}{X_{100} - X_{101}}\right) \quad (4)$$

$$(P_{101}A) = \arctan\left(\frac{Y_A - Y_{101}}{X_A - X_{101}}\right) \quad (5)$$

$$(P_{101}B) = \arctan\left(\frac{Y_B - Y_{101}}{X_B - X_{101}}\right) \quad (6)$$

$$(P_{101}C) = \arctan\left(\frac{Y_C - Y_{101}}{X_C - X_{101}}\right) \quad (7)$$

$$\beta_A = (P_{101}P_{100}) - (P_{101}A) \quad (8)$$

$$\beta_B = (P_{101}P_{100}) - (P_{101}B) \quad (9)$$

$$\beta_C = (P_{101}P_{100}) - (P_{101}C) \quad (10)$$

The above-mentioned stake-out elements are applied by observing at the P.100 control point with a total station set up at point P.101, and these points are evident at the land level.

## 2.2. Computation of the Inner Connection Pathway Curve, Inverted Parietal Deviation Angle, and Development Tail

The deviation angle  $\Delta_1$  of the  $O_1$  center curve and the deviation angle  $\Delta_2$  and the deviation angle  $\Delta_3$  of the  $O_2$  center curve are obtained from the following geodetic equations, taking the coordinates of the points A,  $O_1$ , B, B', C, E, E, and  $O_2$  into account in Fig. 7.

$$\Delta_1 = (O_1A) - (O_1B) \quad (11)$$

$$\Delta_2 = (O_1E) - (O_1B') \quad (12)$$

$$\Delta_3 = (O_2E') - (O_2C) \quad (13)$$

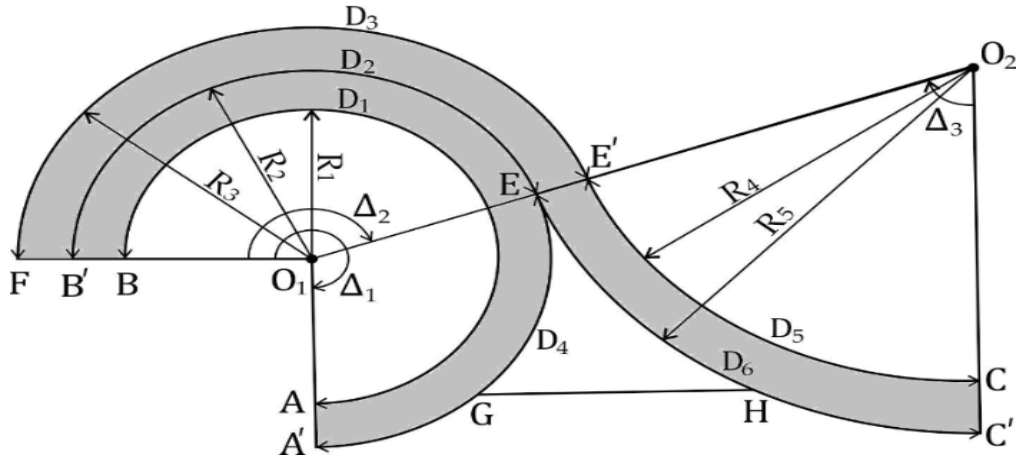


Fig. 7. Geometry of connection paths in the trumpet interchange (inverse curve and inner curve)

$D_1, D_2, D_3, D_4, D_5$ , and  $D_6$  of each curve are computed from the following relation, taking into account the radiuses of the respective curves ( $R_1$ ) and the angles of deviation ( $\Delta_1, \Delta_2$ , and  $\Delta_3$ ) computed by these equations (11), (12), and (13) [7].

$$\text{AB arc length } D_1 = \frac{2 \cdot \pi \cdot R_1}{400} \cdot \Delta_1 \quad (14)$$

$$\text{EB' arc length } D_2 = \frac{2 \cdot \pi \cdot R_2}{400} \cdot \Delta_2 \quad (15)$$

$$\text{A'E arc length } D_4 = \frac{2 \cdot \pi \cdot R_2}{400} \cdot (\Delta_1 - \Delta_2) \quad (16)$$

$$\text{CE' arc length } D_5 = \frac{2 \cdot \pi \cdot R_4}{400} \cdot \Delta_3 \quad (17)$$

$$\text{C'E arc length } D_6 = \frac{2 \cdot \pi \cdot R_5}{400} \cdot \Delta_3 \quad (18)$$

$$\text{C'E arc length } D_6 = \frac{2 \cdot \pi \cdot R_5}{400} \cdot \Delta_3 \quad (19)$$

Fig. 5 also shows that the  $O_2$  center point and radius  $R_4$ ,  $MC = ME'$  tangent length, are computed by using the following equation 20:

$$MC = ME' = R_4 \cdot \tan\left(\frac{\Delta_3}{2}\right) \quad (20)$$

The stake-out (with the polar method) elements of the highway were computed by using the formulas [6].

### 3. Polar Method Stake-out Of Curve Interval Points From Tangential Points

#### 3.1. Land-elevation Stake-out of Curve Interval Points

In general, when the number of intermediate points to be formed in the Stake-out of the spots belonging to the curve is determined, it is desirable that the difference between the spring length determined between the intermediate points of the curtain and the length of the beam length of that spring is not more than 1 cm. For this, for curves with a radius of up to 300 m, the arc length  $\ell^I$  between the two intermediate points can be taken as equation 21:

$$\ell^I \cong \frac{R}{10} \quad (21)$$

Approximate number of intermediate points ( $n'$ ), taking into account the approximate arc height ( $\ell^I$ ) and the curve D development height

$$n' = \frac{D}{\ell^I} - 1 \quad (22)$$

is obtained from the relation. The number of intermediate points is an integer.  $n'$  is rounded by looking at the number after the counting of the fractional number obtained as  $n'$ ,  $n$  is the number of intermediate points. The exact spring length ( $\ell$ ) considering  $n$  and  $D$

$$\ell = \frac{D}{n+1} \quad (23)$$

is obtained from the relation.  $\varepsilon$  angle in the center of the circle of arc

$$\varepsilon = \frac{\ell}{R} \cdot \rho \quad (24)$$

In Fig. 7, in the Stake-out of the interconnection points AB, FE', E'C, and EC'; the exact arc lengths between the intermediate points and the  $\varepsilon$  arcs that see this arc length from the center are calculated by operating in the manner described above. In the Stake-out of the intermediate points of the radius A'B' arc of radius R2, the exact arc length between the intermediate points, and the  $\varepsilon$  angle that sees this arc length from the center must be calculated considering the GB's arc size (gathering D2 and D4 development).

In polar Stake-out of curve points and land and project elevations, usually the tangential point of the curve is taken as the station point, while the connection point is taken as the marked point on the tangent line of the curve.

In Fig. 5,

- For the Stake-out of curve points of the AB spring, A point is taken to the station, G, H, or L' point connection point,
- For the Stake-out of the curve anchor points of A'B', the A point station, C', or L point connection point is taken, and the Stake-out is started from point G,

- For the Stake-out of the curve points of the CE', C point station, H or G point connection point,
- For the Stake-out of the curve points of the C'E arc,
- C point station, A' or K point connection is taken, and Stake-out starts from H point,
- For stake-out of intermediate points of the E'F arc, the Stake-out is initiated by accepting the M' point marked in the extension of the E' point station, E'M.

The Stake-out to be done by the polar coordinate method; for the Stake-out elements  $\epsilon_1, \epsilon_2, \epsilon_3$ ,  $AP_1, AP_2$ , and  $AP_3$  of intermediate points such as a curve  $P_1, P_2, P_3$ :

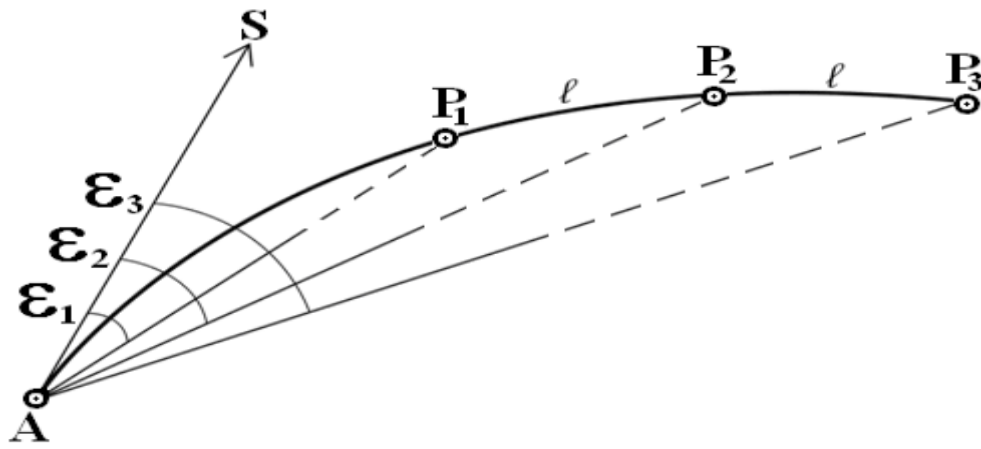


Fig. 8. The polar Stake-out of the intermediate points according to AS tangential direction from point A

$$\epsilon_1 = \epsilon/2 \quad (25)$$

$$\epsilon_2 = 2 \cdot \epsilon/2 \quad (26)$$

$$\epsilon_3 = 3 \cdot \epsilon/2 \quad (27)$$

$$AP_1 = 2 \cdot R \cdot \sin \epsilon_1 \quad (28)$$

$$AP_2 = 2 \cdot R \cdot \sin \epsilon_2 \quad (29)$$

$$AP_3 = 2 \cdot R \cdot \sin \epsilon_3 \quad (30)$$

are used in these relations (Fig. 8), [6, 7].

The Stake-out elements of the curve intermediate points are calculated and applied according to the above-mentioned principles to each curve in connection paths so that the points that make up the connecting roads become apparent at the land level.

#### 4. Results

Numerical data for a highway project related to the subject were generated, including the reverse curve forming the outer part of a trumpet interchange and the project data of the connection path in the form of a circular arc. Since there was no plan for the route on a coordinate map, numerical stake-out was performed. Fig. 5 is taken as an example of a numerical stake-out in relation to the related stake-out, [1]. The radiuses of  $O_1$  center curves are  $R_1 = 40$  m,  $R_2 = 45$  m, and  $R_3 = 50$  m, and the radiuses of  $O_2$  center curves are  $R_4 = 55$  m and  $R_5 = 60$  m.

The road design subject to the stake-out is transferred to a computer environment with computer hardware. The marked points (A, A', B, B', C, C', E, E', F, G, H, K, L, K', L',  $O_1$ ,  $O_2$ ) in the highway map are digitized, and P.101 is the station point and P.100 is the connection point. Stake-out elements are calculated and applied at the heights of B, B', E, E', F, and G points. It has been applied that the A, A', C, C', H, K, L, K', and L points are applied at project height.

Using the coordinates of the digitized A,  $O_1$ , B, B', C, E, E', and  $O_2$  points in Fig. 5, the divergence angle of  $\Delta_1$  was 300g.0120, the divergence angle of divergence was 181g.0220, the divergence angle was 76g.2250 were obtained from (11), (12), and (13) equations. From the data received from the project of the trumpet interchange, It is assumed to be  $\Delta H_{AB}=8.50$  m,  $\Delta H_{A'B'}=8.60$  m,  $\Delta H_{E'F}=8.50$  m,  $\Delta H_{CE}=2.72$  m,  $\Delta H_{C'E}=2.82$  m.

Table 1. The data on the development of the curves, the approximate and precise number of points, the exact arc length, and the angles that see these springs from the center

Centre of the curve	The divergence angle $\Delta_i$	R Radius (m)	Development length (m)	Approximate number of waypoints (n')	The exact number of waypoints (n)	Definite intermediate spring length ( $\ell$ )	$\ell$ angle seen from the centre ( $\epsilon$ )
$O_1$	300g.0120	40	$D_1=188.503$	46.12	46	4.0110	6.3832
$O_1$	181g.0220	45	$D_2=127.957$	46.12	46	4.5120	6.3832
$O_1$	118g.9900	45	$D_4= 84.109$	-	-	-	-
$O_1$	181g.0220	50	$D_3=142.174$	27.44	27	5.0770	6.4650
$O_2$	76g.2250	55	$D_5= 65.854$	10.97	11	5.4878	6.3521
$O_2$	76g.2250	60	$D_6= 71.840$	10.97	11	5.9867	6.3521

Using project data and the relevant relativity, the development tiles of the curves forming the external and internal connection at the trumpet interchange, the approximate and precise number of points, the exact arc lengths ( $\ell$ ), and the angles ( $\epsilon$ ) are calculated and shown in Table 1.

Table 2. Calculation slopes, slope angles, and vertical angles of the curves forming the connecting path

Curve	Relevant arc	D (m)	Height difference	Slope	Slope angle $\alpha$	Vertical angle Z
$O_1$ center $R_1$ radius	AB	188.503	8.50	0.04509212	2.8687	97.1313
$O_1$ center $R_2$ radius	A'B'	212.066	8.60	0.04055340	2.5803	97.4197
$O_1$ center $R_3$ radius	E'F	142.174	6.41	0.04508560	2.8649	97.1351
$O_2$ center $R_4$ radius	CE'	65.854	2.72	0.04130350	2.6280	97.3720
$O_2$ center $R_5$ radius	C'E	71.840	2.82	0.03925390	2.4977	97.5023

Considering the height differences between the points where the connecting roads are tangent to the upper and lower main ties and the development tile, the calculated slope angles ( $\alpha$ ) and vertical angles ( $Z$ ) are shown in Table 2.

Table 3. The stake-out elements for the stake-out of the intermediate points at the land height and the project height with center O1R1 = 40 m and radius  $\Delta 1 = 300$  g.0120

Station Point	Point of	Horizontal angle ( $\epsilon_i$ )	Horizontal distance ( $\Delta i$ )	Length of spring $A_i$ ( $\ell_i$ )	The slope of the road	Project Height	Vertical angle	Height of reflector
A	H	0.0000				$H_A=0.00$		1.52
a=1.52	1	3.1916	4.009	4.011	0.0450921	0.181	97.1313	“
	2	6.3832	8.008	8.022	“	0.362	“	“
	3	9.5748	11.987	12.033	“	0.542	“	“
	4	12.7664	15.935	16.044	“	0.723	“	“
	5	15.9580	19.844	20.055	“	0.904	“	“
	6	19.1496	23.703	24.066	“	1.085	“	“
	7	22.3412	27.502	28.077	“	1.266	“	“
	8	25.5328	32.232	32.088	“	1.447	“	“
	9	28.7244	34.884	36.099	“	1.628	“	“
	10	31.9160	38.448	40.110	“	1.808	“	“
	11	35.1076	41.915	44.121	“	1.989	“	“
	46	146.8144	78.120	184.503	“	8.320	“	“

Using the data in Table 1 and Table 2, the stake-out elements calculated both at the grade level and the project level are shown in Tables 3, 4, 5, 6, and 7. Since the deviation angle of the curve with center  $O_1$  and radius  $R_1$  is 300g.0120, the number of curve intermediate points located between the tangent points A, B, and A', B' is too high (46), the application elements of the first 11 and the last intermediate point are calculated in Table 3 and are shown in Table 4.

On the other hand, the first 11 of the 27 intermediate points belonging to the curve with a center of  $O_1$  and a radius of  $R_3$  with a declination angle of 181g.0220 are calculated and shown in Table 5.

$$E'M = MC = R_4 \cdot \tan \frac{\Delta_3}{2} = 40.931 \text{ m} \quad (31)$$

Table 4. The Stake-out elements required for the Stake-out of the intermediate points at the land height and the project height with center O1R1 = 45 m and radius  $\Delta 1 = 300$ g.0120

Station Point	Point of	Horizontal angle ( $\epsilon_i$ )	Horizontal distance ( $\Delta i$ )	Length of spring $A_i$ ( $\ell_i$ )	The slope of the road	Project height	Vertical angle	Height of reflector
A'	C'	0.0000				$H_A=0.00$		1.54
a=1.54	1	3.1916	4.510	4.512	0.040553	0.183	97.4197	“
	2	6.3832	9.008	9.024	“	0.366	“	“
	3	9.5748	13.485	13.536	“	0.549	“	“
	4	12.7664	17.927	18.048	“	0.732	“	“
	5	15.9580	22.324	22.560	“	0.915	“	“
	6	19.1496	26.666	27.072	“	1.097	“	“
	7	22.3412	30.940	31.584	“	1.281	“	“
	8	25.5328	35.136	36.096	“	1.464	“	“
	9	28.7244	39.244	40.608	“	1.647	“	“
	10	31.9160	43.254	45.120	“	1.830	“	“
	11	35.1076	47.154	49.632	“	2.013	“	“
	46	146.8140	87.886	207.552	“	8.417	“	“



The point M, which has a horizontal length of  $E'M=MC=40,931$  m from C, is marked in the direction of CH in the field. With the electronic tachometer installed at the E' point, the M point is looked at, the binoculars are rolled up, and the M' point is marked in the direction in which the binoculars are directed. E'M' direction is taken as the tangent direction of the stake-out of the intermediate points of the E'F circle arc.

Table 5. The stake-out elements for the stake-out of the intermediate points at the land height and the project height with center  $O_1R_1 = 50$  m and radius  $\Delta_1 = 181g.0220$

Station Point	Point of	Horizontal angle ( $\epsilon_i$ )	Horizontal distance ( $A_i$ )	Length of spring $A_i$ ( $l_i$ )	The slope of the road	Project height	Vertical angle	Height of reflector
E'	M'	0.0000				$H_{E'}=0.0$		1.55
a=1.55	1	3.2325	5.075	5.077	0.0450856	0.229	97.1351	“
	2	6.4650	10.138	10.154	“	0.458	“	“
	3	9.6975	15.174	15.231	“	0.687	“	“
	4	12.9300	20.171	20.308	“	0.916	“	“
	5	16.1625	25.116	25.385	“	1.144	“	“
	6	19.3950	29.996	30.462	“	1.373	“	“
	7	22.6275	34.800	35.539	“	1.602	“	“
	8	25.8600	39.513	40.616	“	1.831	“	“
	9	29.0925	44.124	45.693	“	2.060	“	“
	10	32.3250	48.622	50.770	“	2.289	“	“
	11	35.5575	52.994	55.847	“	2.518	“	“

Table 6. The Stake-out elements required for the Stake-out of the intermediate points at the land height and the project height with center  $O_1R_1 = 55$  m and radius  $\Delta_1 = 76g.2250$

Station Point	Point of	Horizontal angle ( $\epsilon_i$ )	Horizontal distance ( $A_i$ )	Length of spring $A_i$ ( $l_i$ )	The slope of the road	Project height	Vertical angle	Height of reflector
C	H	0.0000				$H_C=0.00$		1.51
a=1.51	1	3.1760	5.486	5.4878	0.0413035	0.227	97.3720	“
	2	6.3521	10.957	10.976	“	0.453	“	“
	3	9.5282	16.402	16.463	“	0.680	“	“
	4	12.7042	21.806	21.951	“	0.907	“	“
	5	15.8802	27.155	27.439	“	1.133	“	“
	6	19.0563	32.437	32.927	“	1.360	“	“
	7	22.2323	37.639	38.415	“	1.587	“	“
	8	25.4084	42.746	43.903	“	1.813	“	“
	9	28.5844	47.747	49.390	“	2.040	“	“
	10	31.7605	52.630	54.878	“	2.267	“	“
	11	34.9366	57.381	60.366	“	2.493	“	“

Table 7. The Stake-out elements required for the Stake-out of the intermediate points at the land height and the project height with center  $O_1R_1 = 60$  m and radius  $\Delta_1 = 76g.2250$

Station Point	Point of	Horizontal angle ( $\epsilon_i$ )	Horizontal distance ( $A_i$ )	Length of spring $A_i$ ( $\ell_i$ )	The slope of the road	Project Height	Vertical angle	Height of reflector
C'	A'	0.0000				$H_C=0.00$		1.52
a=1.52	1	3.1760	5.984	5.9867	0.0392539	0.235	97.5023	"
	2	6.3521	11.953	11.973	"	0.470	"	"
	3	9.5281	17.893	17.960	"	0.705	"	"
	4	12.7041	23.788	23.947	"	0.940	"	"
	5	15.8801	29.624	29.933	"	1.175	"	"
	6	19.0562	35.386	35.920	"	1.410	"	"
	7	22.2322	41.060	41.907	"	1.645	"	"
	8	25.4082	46.632	47.893	"	1.880	"	"
	9	28.5842	52.087	53.880	"	2.115	"	"
	10	31.7602	57.414	59.867	"	2.350	"	"
	11	34.9363	62.597	65.853	"	2.585	"	"

## 5. Conclusions

This study examined the polar stake-out of the curves in the trumpet intersection's connection road.

First of all, the entry and exit points and tangent points of the connection roads to the main roads should be stake-out according to the criteria specified in the article.

Internal and external connection roads: Since there are roads where vehicle speed is generally reduced, slope application is not needed. If slope is required in the intersection project, the stake-out of the points on the right and left of the connection road axis should be made according to the height values calculated according to the project slope.

In order to prevent the vehicle from crossing into the opposite lane in case of a traffic accident, metal guardrails are placed on both sides of the connection road. The guardrail points to be built on the right and left borders of the road should also be staked out.

Before the connecting road at different level crossings, after the connection highway has been made roughly by filling the curved intermediate points marked temporarily at the land level, the stake-out should be made at the project level of the intermediate points by installing tools again at the relevant tangent points.

Trumpet interchange is used in road applications in urban and non-residential areas. In this study, how to stake-out these intersections is explained in detail.

## Author Contribution

Mehmet Eren: Conceptualization, Software, Writing, Investigation.

Aziz Uğur Tona: Methodology, Review & Editing, Writing, Supervision.

## References

- [1] AASHTO, *A Policy on Geometric Design of Highways and Streets*, ISBN: 978-1-56051-676-7, Chapters 9.1-174/10.10-157, 2018


- [2] Lay, M. G., Handbook of Road Technology, 4th ed., Spoon Press, New York, USA, 516-517, 2009. <https://doi.org/10.1201/9781482288667>.
- [3] Yalçın, E.G., Characteristics of Cloverleaf Interchange in Turkey, MS Thesis, METU The Graduate School of Natural and Applied Sciences, 1–11, 2018. <https://hdl.handle.net/11511/27894>.
- [4] Abakan, A.O., Safety Analysis of Interchange Functional Areas, Iowa State University Graduate Thesis and Dissertations, 15479, 13–17, 2017.
- [5] Allan, A. L., Principles of Geospatial Surveying, Whittles Publishing, 241-244, 252-254, 2007. ISBN : 978-184995-145-6
- [6] Ghilani, C. D., Wolf, P. R., Elementary Surveying: An Introduction to Geomatics, 13th ed., Pearson Prentice-Hall, Upper Saddle River, New Jersey, ISBN: 978-13-255434, 277-287, 715-755, 2012.
- [7] Kavanagh, B.F., Surveying Principles and Applications, Pearson Education, Inc., Prentice Hall, Upper Saddle River, ISBN : 9780132365123, 504-525, 2009.
- [8] McCormac, J.C., Surveying Fundamentals, 2nd ed., Prentice Hall, USA, ISBN: 0-13-878843-X, 451-482, 1983/2012.
- [9] Schofield, W., Breach, M., *Engineering Surveying*, 6th ed., Butterworth Heinemann, Oxford, ISBN: 978-0750-669498, 189-318, 370-391, 2007.
- [10] Sestras, P., Methodological and On-Site Applied Construction Layout Plan with Batter Boards Stake-Out Methods Comparison: A Case Study of Romania, *Applied Sciences*, 11(10), 4331, 2021. doi:10.3390/app11104331.
- [11] Cosarca, C., Considerations on Tolerances and Precisions in Engineering Cosarca, C. Considerations on tolerances and precisions in engineering measurements. In Recent Advances in Geodesy and Geomatics Engineering-Proceedings of the 1st European Conference of Geodesy Geomatics Engineering; Technical University for Civil Engineering Bucharest: Bucharest, Romania, 2013, 1, 8–18. ISBN: 978-960-474-335-3.
- [12] Matei, I., Pacurar, I., Rosca, S., Bilasco, S., Sestras, P., Rusu, T., Jude, E.T., and Tăut, F.D., Land Use Favourability Assessment Based on Soil Characteristics and Anthropic Pollution. Case Study Somesul Mic Valley Corridor, Romania, *Agronomy*, 10, 1245, 2020. <https://doi.org/10.3390/agronomy10091245>.
- [13] Kavanagh, B. F., Slattery, D. K., Surveying: With Construction Applications, Pearson, Upper Saddle River, NJ, USA, 2010. ISBN: 978-0-13-500051-9.
- [14] Coșarcă, C., Măsurători Inginerești: Aplicații în Domeniul Construcțiilor, 1st ed., Matrix, Bucharest, Romania, ISBN: 9789737557155, 22–93, 2011.
- [15] Schofield, W., Engineering Surveying: Theory and Examination Problems for Students, Elsevier, London, UK, 2001. ISBN: 0-7506-4987-9.
- [16] Google Earth Website: <http://earth.google.com/web/> (Access Date: 03.04.2024)
- [17] İnce, H., A New Relation Developing on Stake-out of Curve Intermediate Points by Method of Sequential Tangents, 5. National Engineering Surveying Symposium, Notice Book, (Turkish mean), 547-553, 2010.

## Investigating Solar Energy Potential in Afghanistan under Certain Climatic and Geometrical Parameters of Cities and Buildings

Edris Naseri <sup>a\*</sup>, Burcin Deda Altan <sup>b</sup>, Afsin Gungor <sup>c</sup>

<sup>a</sup>, Department of Mechanical Engineering, Institute of Natural and Applied Sciences, Akdeniz University, Antalya, Turkey

<sup>b,c</sup> Department of Mechanical Engineering, Faculty of Engineering, Akdeniz University, Antalya, Turkey

✉: [naseri6341@gmail.com](mailto:naseri6341@gmail.com) <sup>a\*</sup>, [bdeda@akdeniz.edu.tr](mailto:bdeda@akdeniz.edu.tr) <sup>b</sup>, [afsingungor@akdeniz.edu.tr](mailto:afsingungor@akdeniz.edu.tr) <sup>c</sup>, : 0009-0001-4121-3665<sup>a\*</sup>, 0000-0001-6834-9215<sup>b</sup>, 0000-0002-4245-7741 <sup>c</sup>

Received: 10.10.2024, Revised: 3.12.2024, Accepted: 6.12.2024

### Abstract

Afghanistan faces significant challenges in meeting its growing energy demands, with the building sector consuming a substantial portion of its energy supply. The country increasingly turns to solar energy as a clean and sustainable alternative to address these challenges. While previous studies have explored solar energy potential in Afghanistan, there is a lack of comprehensive research focusing on building sector applications and the interplay of climatic and geometrical factors. This study aims to assess the potential of solar energy for the building sector in Afghanistan by examining the influence of climatic and geometrical factors. A systematic literature review was conducted to identify existing research and data on solar energy resources, building characteristics, and energy consumption patterns. The findings reveal that Afghanistan possesses substantial solar energy potential, particularly in the southwest and west regions. Building orientation, insulation, and shading are identified as crucial factors influencing solar energy performance. By exploring the suitability of various solar technologies, including solar photovoltaic, solar thermal, and solar lighting systems, this research contributes to the knowledge base on solar energy in Afghanistan. It provides insights for policymakers and practitioners seeking to promote sustainable building practices.

**Keywords:** Afghanistan, solar asset, building energy, solar energy, geometrical parameters.

### 1. Introduction

Afghanistan (AFG) is facing a profound energy crisis, characterized by a persistent energy deficit, unreliable electricity supply, and a rapidly increasing demand for energy, particularly in the building sector. The country's heavy reliance on imported electricity and fossil fuels, coupled with a rapidly expanding population, has exacerbated these challenges. The lack of access to reliable electricity hinders economic growth, social development, and quality of life. Solar energy (SE), with its abundant availability and minimal environmental impact, offers a sustainable and viable solution to Afghanistan's energy challenges. Harnessing solar power has the potential to reduce the country's reliance on fossil fuels, mitigate greenhouse gas emissions, and enhance energy security. However, the full potential of solar energy in Afghanistan has yet to be realized, particularly in the building sector.

Access to power energy is the top priority for Afghan homes and businesses after security. During 2005–2012, energy consumption grew at more than double the pace of economic growth. Conversely, Afghanistan has one of the lowest per capita energy consumption rates in the world and is a net energy importer. More than 80% of the country's overall power supply comes from neighboring nations, with the balance coming from hydroelectric and thermal power plants. Afghanistan's energy security is still hampered by a lack of local power

generation. Afghanistan is a geography that has hot summers and chilly winters, the country's climate is marked by intense solar radiation and long hours of sunlight [1].

Solar energy is extensively considered to be a sustainable and easily available energy source in the building sector. According to a United Nations report, 55% of the world's population resides in downtowns, as they consume a large amount of energy and generate enormous global carbon emissions simultaneously. In particular, urbanization shifts gradually in the residence of the human population from rural to urban areas, and that is expected to increase to 68% by 2050 [2]. Air pollution in the building sector is a significant worldwide concern in developed and developing countries. The swelling of the urban population density in cities, pollution emissions increase, and air pollution aggravates that effect on the environment and human health[3]. Hence, air quality in cities should be considered urgently, and factors that can exacerbate air pollution sources should be controlled to improve national health levels. This leads to the need to use solar energy to reduce the effects of fossil fuel consumption and improve the quality of life of society [4].

Buildings are the main component in the fabric of cities. Also, the building and construction sector is one of the most significant areas of intervention, providing opportunities to limit environmental impacts and help achieve sustainable development goals. It has been estimated that the building sector comprises one-third of energy-related greenhouse gas (GHG) emissions [5] and these factors combine to make the building sector one of the largest energy consumers in the world [6]. Moreover, solar energy brings several benefits both economically and environmentally because it preserves the ecosystem [7]. As a result, solar energy might be considered a viable alternative source of sustainable energy in the construction industry. The number of solar concentrating systems for building integration has expanded dramatically in recent years, as these systems are more efficient in terms of space consumption than typical flat modules [8]. Significant growth can be expected in building energy consumption, which includes electrical power, heating, and cooling, etc.

Afghanistan's energy sector has notable obstacles, such as a major dependence on imports, a rapid increase in energy consumption, and a significant demand for energy in the building sector [9]. Although the country possesses vast solar resources [10], it has not fully used this potential to meet its energy requirements [11]. This study aims to examine the feasibility of incorporating solar energy into the building sector in Afghanistan by studying how climatic and geometric elements interact.

Although previous research investigated Afghanistan's overall capacity for solar energy, there is a lack of thorough knowledge regarding its specific use in the construction industry. This review aims to fill this gap by analyzing the current collection of information on solar energy resources, building attributes, and energy usage patterns in Afghanistan. This research enhances the development of sustainable and resilient building practices in the country by identifying the most appropriate solar technologies and investigating their integration into the building structure. This study concentrates on the application of solar energy in the building sector of Afghanistan, going beyond earlier research that has only investigated the general possibilities of solar energy. This review seeks to comprehensively examine the viability of various solar technologies for different building typologies in Afghanistan by examining climatic and geometrical parameters.

This paper is structured as follows: Section 3 provides a comprehensive overview of AFG's climatic and geographical conditions, and essential factors influencing SE potential. Section 4 explores global energy trends to provide a broader context for AFG's energy challenges. Section 5 delves into the country's energy demand, with a particular focus on the building sector.

Building characteristics and the potential integration of SE systems are analyzed in Section 6. Section 7 provides a forum for discussion, analyzing critically how well SE works to address the issues of AFG's energy challenges. Finally, Section 8 summarizes the findings, and outlines potential avenues for future research.

## **2. Methodology**

This review employed a systematic literature review approach to investigate the potential of SE in AFG's building sector. The following steps were undertaken:

### **Literature Search**

A comprehensive literature search was conducted using Google Scholar, Scopus, and Web of Science. Keywords such as "Afghanistan," "solar energy," "building," "climatic factors," and "geometrical parameters" were used to identify relevant studies. The search was limited to peer-reviewed articles published in English and the local language.

### **Inclusion and Exclusion Criteria**

Studies were included if they:

- Focused on SE in AFG.
- Addressed the building sector and its energy needs.
- Provided quantitative or qualitative data on SE potential, climatic conditions, or building characteristics.

Studies were excluded if they:

- Lacked sufficient methodological rigor or data.
- Were primarily opinion-based or anecdotal.

### **Data Extraction**

Relevant data, including author(s), publication year, journal, study design, methodology, key findings, and conclusions, were extracted from the selected studies using a standardized data extraction form.

### **Data Analysis**

A qualitative thematic analysis was conducted to identify key themes and patterns in the literature. Quantitative data, where available, was analyzed using descriptive statistics and statistical software.

### **Limitations**

The limitations of this review must be acknowledged. This may have affected the depth of study because there is a dearth of detailed data on SE in AFG. Also, it's possible that pertinent studies written in other languages were overlooked due to the concentration on English and regional publishing. Taking into account the impact of geometrical and climatic factors, this review attempts to offer a thorough and perceptive summary of the SE potential in AFG's building industry by employing a methodical methodology.

## **3. The Geography and Climate of Afghanistan**

AFG is located in Central Asia [12], and it is a landlocked and mountainous country [1, 13]. The geography of AFG includes irrigation areas, small but fertile river valleys, deep gorges, deserts, highlands, and snow-capped mountains. The eastern part of the country is divided by the towering Hindu Kush and Pamir mountains which rise to around 7500 meters [14]. The



land of AFG is very different and by crossing the lower central mountains, to the high mountains in the northeast, it is going from the deserts of the Kandahar region in the West to the Turkestan plains in the North [13]. About 73% of AFG is savannah, shrubbery and meadow, while 15% is snow and ice alongside sparse or barren vegetation [15].

The performance of solar systems depends on local climatic conditions. The climate in AFG, however, varies significantly across provinces. Most parts of the country have an arid or semiarid continental climate and the variance in terrain and elevation results in different climatic types [1]. AFG with hot summers and cold winters has although high air turbidity. In the summertime, the high temperature frequently exceeds 38°C in the Southwest region, while wintertime lows can reach below -25°C [16]. Elevations and air turbidity suggest high renewable resources [17].

#### 4. Global Energy Scenarios

The global energy landscape is undergoing significant transformation, driven by factors such as population growth, economic development, and climate change. While renewable energy (RE) sources, particularly solar and wind, are gaining prominence, fossil fuels continue to dominate the global energy mix. The latest reports in the energy sector mark a major change in the energy sector in the coming decades. For instance, the Government of India reports that more than 99 % of the population has access to electricity, and useful and operative policies are being implemented in some countries in Africa. Also, the assessments show that about 2.6 billion people did not have access to clean cooking and 770 million people did not have connected to electricity in 2019 [18].

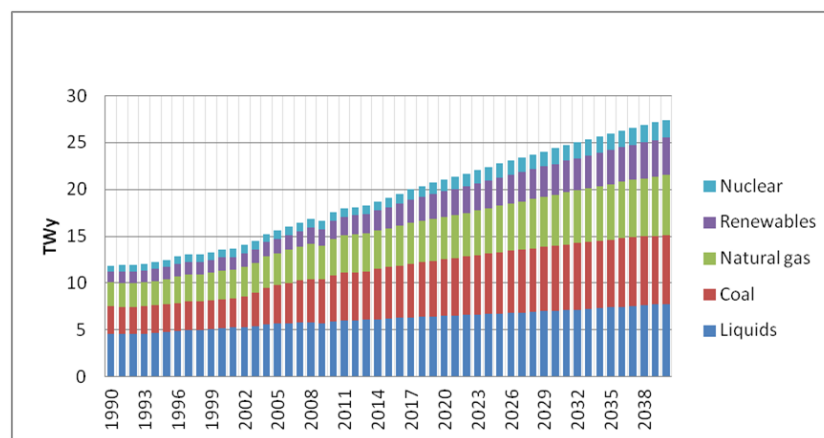


Fig. 1. EIA World energy consumption projection by fuel type

The increase in energy demand is proportional to population growth [19] as a result the global primary energy consumption increased from 270.5 EJ in 1978 to 580 EJ in 2018, more than doubled. In the past 40 years, fossil fuels mostly covered the total world energy consumption and the contribution of fossil fuels was 7 % less in 2018 than in 1978 [20]. Globally, as indicated in Fig. 1, by 2040 renewables still provide less than 5 % of the global energy demand. Fossil fuels (coal, oil, and natural gas) continue to dominate [21].

The global energy transition offers both challenges and opportunities in AFG. The country's energy demand is rapidly increasing, driven by population growth and economic development. However, AFG faces significant challenges in meeting this growing demand, including a lack of infrastructure, political instability, and a reliance on imported electricity and fossil fuels.

By leveraging its abundant solar resources, AFG can reduce its dependence on fossil fuels, improve energy security, and contribute to global efforts to mitigate climate change. Integrating SE into the country's energy mix can provide a sustainable and cost-effective solution to its energy challenges.

## **5. Energy Demand in Afghanistan**

Access to safe energy resources in AFG has been virtually disrupted due to three decades of wars [2]. Most of the electricity generation, transmission, and distribution infrastructure was destroyed and the remaining facilities were very, very small [22]. In 2001, less than 5 % of the country's population had access to electricity, while in 2015 the figure rose to 30 % [23]. AFG has one of the lowest electricity consumption in the world, consuming 119.8 kWh per capita [12].

Recently, the development of electricity capacity in AFG has depended on imports of energy from neighboring countries. In 2011, about 80 % of the country's total electricity was imported from Uzbekistan [22]. In 2015, the capacity of electricity generation inside AFG was about 1000 gigawatts/hour (GWh), which was 22 percent of the total electricity consumption [23]. Hence, in the Power Sector Master Plan of the government, electricity consumption is considered to grow at the rate of 8.7 % per year through 2032 [24].

There are enough fossil fuels and RE in AFG. About 80 million barrels of oil reserves, 75 billion cubic meters of natural gas, 440 billion cubic meters of unspecified natural gas, and 73 million tons of coal reserves have been identified [23]. However, energy production from renewable sources is estimated at 318 GW [25], which is why the largest share of AFG's energy generation is expected to come from RE sources. The enormous wind power potential in AFG can help the South Asian region take a big step forward in meeting its energy needs [12].

Mohammad, Shrestha [26] calculated the urban residential energy use in Kandahar, AFG. This study is based on a survey conducted in the third quarter of 2011 in 10 districts of Kandahar city. Analysis shows that around 72 % of total residential energy is used for cooking, and firewood is still the main form of energy, with a share of around 58 %. The amount of energy consumed in the housing sector has a major share in the total energy consumed in the cities of AFG.

## **6. Buildings & Solar Energy Systems**

The buildings and buildings construction sectors combined are considered as the main driver of energy consumption and GHG emissions in the world. Buildings consume about 40 % of global energy, and the world's total energy demand in residential areas reached 86.8 EJ in 2010 [27]. The share of energy consumption by residential sectors in AFG accounts for 54 % of total consumption [26], and the consumption varies significantly across provinces. Electric grid accessibility and residential facilities affect annual consumption and it ranges from a low value of 178 kWh/household in Ghor and 551 kWh/household in Laghman, to a higher value in urban centers such as Kabul 3,000 kWh/ household and Herat 2,600 kWh per household [28]. Hence, in the Power Sector Master Plan of the government, annual electricity consumption is considered to be 1500 KWh/household through 2032 [28].

Solar radiation is considered to be a primary source of energy for many human activities [29]. The application of SE in buildings discusses the successful utilization of the Sun's energy in the building industry and related fields [30]. In AFG, the main uses of SE in buildings are solar

water heaters, solar cookers, solar pumps, and photovoltaic PV systems. Interestingly, with the inadequacy of local electricity grids and rapidly rising electricity prices, the utilization of SE in the building industry is accelerating. This is due to its potential availability and safe use for small and large scales by residential and commercial buildings (Fig. 2.).

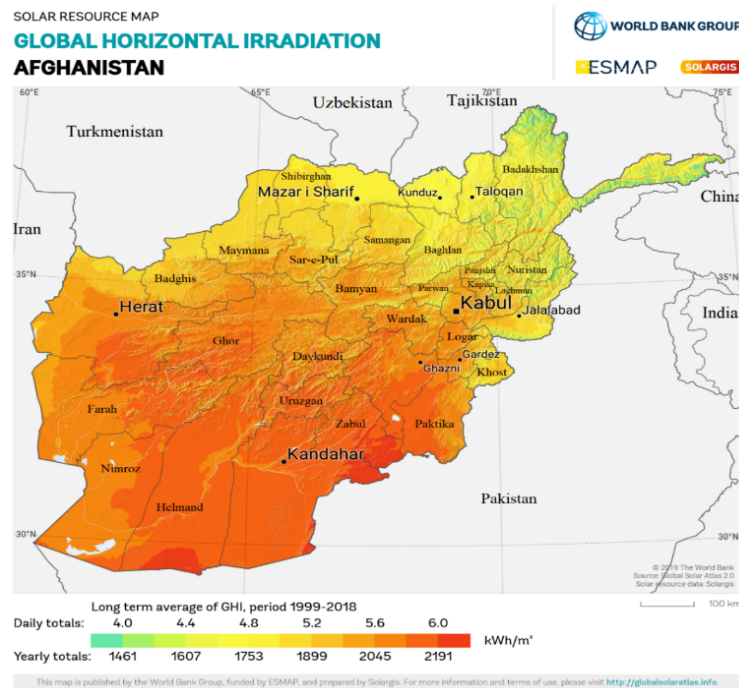


Fig. 2. Horizontal Irradiation, AFG [47]

## 6.1. Solar Assets

The intensity of SE is approximately  $1370 \text{ W/m}^2$  outside of the earth's atmosphere. The amount of incoming solar radiation or insolation that AFG receives is primarily a function of its latitude and most of AFG lies between a latitude of 29 and 38 degrees north [16]. AFG occurs in the subtropical and arid regions of southwest Asia [1]. In summer the northern hemisphere is tilted towards the sun and the periods of daylight are longer. This leads to high temperatures across the country where the maximum daily temperature is above  $38^\circ\text{C}$ . Differences in temperatures occur in winter when the sun sinks to the horizon and the length of the day shortens. As a result, the country acquires a relatively high degree of solar radiation in summer and a low degree of solar radiation in winter [16].

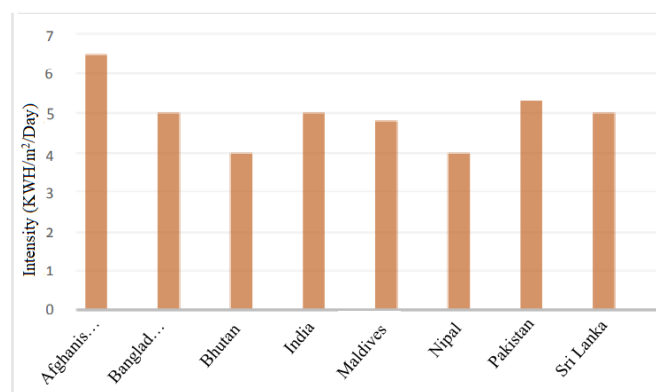


Fig. 3. Average Solar Power Potential of South Asian Countries [31]

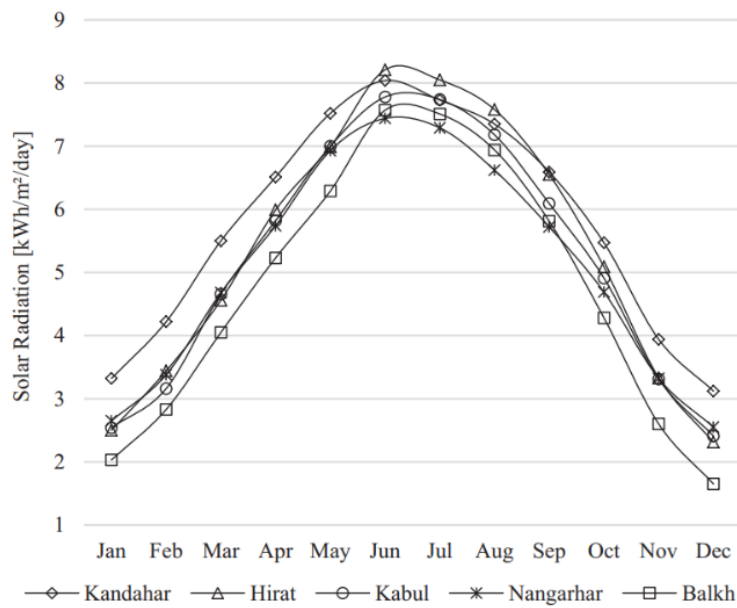


Fig. 4. Monthly GHI of major cities in AFG [34]

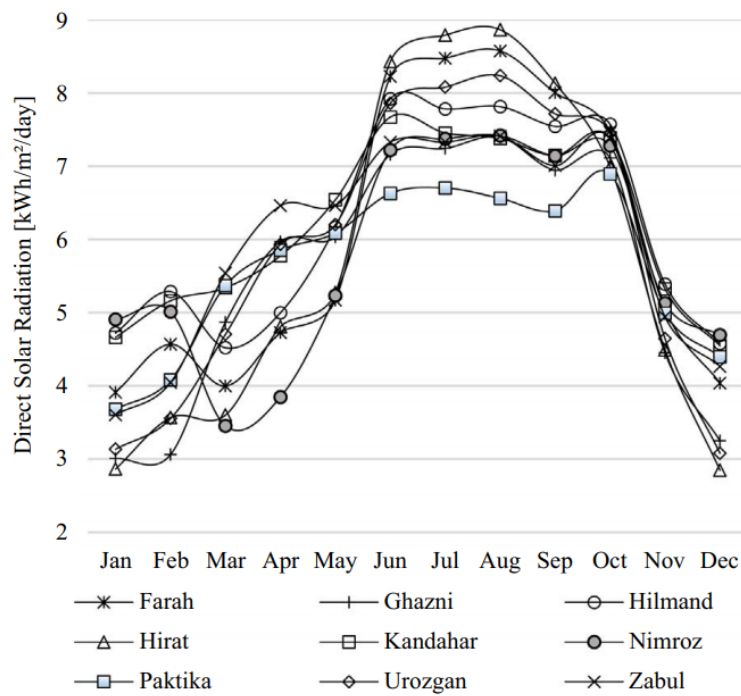


Fig. 5. DNI of CSP areas in AFG [34]

AFG with hot summers and cold winters has although high air turbidity and the climate of the country is characterized by strong solar radiation and huge sunshine hours (more than 3000 hours annually) [1] and more than 300 sunny days per year. Fig. 3 shows the average solar power potential of South Asian Countries [31]. As result, the average solar potential Global Horizontal Irradiance (GHI) is estimated at 6.5 kWh per m<sup>2</sup> per day [12]. Hence, the energy production from SE is 220 gigawatts [23] and the government aims to produce 5,000 megawatts of RE by 2032, which corresponds to 95 % of the country's electricity demand [32].

The U.S. National Renewable Energy Laboratory (NREL) has recently produced high-resolution satellite-derived SE resource maps and related data products for AFG, and the data was included in a geospatial toolkit. Users can manipulate the resource information along with country-specific geospatial information and then transfer resource data for specific locations [33]. NREL produced datasets in a gridded format and with a ground resolution of  $0.1^\circ$  latitude and  $0.1^\circ$  longitude ( $8.5 \text{ km} \times 10 \text{ km}$ ). Irradiance datasets include monthly averages over three years from 2002 to 2005 [24]. NREL provided data for different provinces of AFG that have been analyzed and compared with meteorological measurements at each site as shown in Fig. 4 & Fig. 5.

## **6.2. Solar Potential in the Building**

The life of the people of AFG, in terms of important geographical location, has been influenced by the cultures and arts of different ethnic groups, and this impact has been accompanied by observation and understanding of aesthetics, including the art of architecture. This is seen in the architecture of cities, mosques, houses, and other buildings.

The estimation of surface solar irradiation is very important for many different solar applications. Thousands of domed houses and monuments are located in the cities and villages of AFG, each of which has its value and importance, and archaeologists consider it a valuable treasure of antiquities and historical monuments. Faghih and Bahadori [35] analyzed the solar radiation on domed roofs. Four domed roofs received and absorbed solar radiation at the same rate as a flat roof, and the roofs all had the same base area. As a result, domed roofs received far more solar radiation than flat roofs.

Urban morphology is the analysis of the abstract form of the existing reality [36]. Taking into account the optimal combination of morphological parameters, the solar radiation of ceilings and facades can increase by 9 % and 45 % respectively [37]. Poon, Kämpf [38] performed a parametric study of URBAN morphology on building SE potential in the Singapore context. The researchers discovered a link between urban morphology and yearly average irradiance on rooftops and façades. They considered two multilinear regression predictive models for rooftop and façade and 10 morphology in parameters to compare the correlation performance of building irradiance with the two definitions of the Sky View Factor (SVF). The analysis shows that the correlation performance of the two SVF definitions is the strongest ( $r = 0.94$  to  $1$ ), while  $R^2$  for the rooftop irradiance model ( $R^2 = 0.61$ ) and other individual parameters ( $R^2 = 0$  to  $0.36$ ).

Li, Ding [39] estimated the SE potential on building roofs. This study considers several flat-roofed buildings in the town planning of Xiuyuan eco-city as a study area for measuring solar potential on the roofs of buildings. This study was conducted with a pixel-based methodology. The solar radiation in a given cell is mathematically formulated in pixels, and its yields over a given period are immediately calculated by taking into account a few solar irradiances and presented by visual image processing. Analysis shows that the maximum and minimum annual radiation yields are  $4717.72 \text{ MJ/m}^2$  and  $342.58 \text{ MJ/m}^2$  respectively. Hence, 20 % of the roof areas of each building can obtain  $4500 \text{ MJ/m}^2/\text{year}$  or more solar radiation.

Kanters and Horvat [40] demonstrated the exploration of geometric shapes of urban blocks and the potential of SE for local energy production. They performed the Simulations with the Ecotect program for the city of Lund, in southern Sweden. This study showed that the impact of the geometric shape on the SE potential can be up to twice and some shapes are less sensitive

to different orientations. In dense cities, when buildings are surrounded by another geometry, the share of SE decreases by 10 to 75 %.

### 6.3. Utilization of Solar Energy in Buildings

The concept of harnessing the power of the sun was common practice even thousands of years before the era of solar panels. Although SE plays a dynamic and fundamental role in today's power potential, the use of SE for water heating, light fires, sunrooms, and drying crops has had a tradition in the past, so there is a long history behind PV that embodies the concept of SE. Solar panels provide clean energy [4]. There are no harmful GHG emissions in the process of PV energy production, therefore solar PV energy is environmentally friendly [7].

There are many applications of SE such as light-gathering, SE photo-thermal, and PV utilization which is cost-effective, particularly for the AFG building industry. Yang, He [41] analyzed the application of solar technologies in building energy efficiency. Meanwhile, they showed that photo-thermal technology is suitable for solar-powered residential buildings in comparison with the light-gathering utilization, and PV utilization in terms of technology and current economy.

#### 6.3.1 Solar thermal utilization

Concentrating solar thermal technologies collect and concentrate solar radiation to convert it into thermal energy at high temperatures as shown in Fig. 7. [42]. This thermal energy is then transmitted via a transport medium or moving fluid for domestic use. In AFG, the building sector uses local coal, fuel wood, and liquefied petroleum gas (LPG) as part of its energy mix. AFG's energy production and supply are highly volatile, as is the country's reliance on imported petroleum products. Therefore, concentrating solar thermal technologies can be efficient for a wide variety of AFG building sector applications, including heating and cooling, process heating, and power generation.

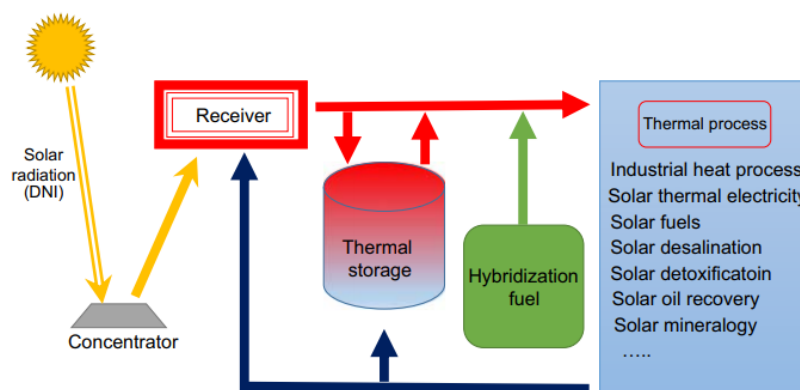


Fig. 6. General scheme of a concentrating solar thermal system [42]

With a payback period of 7-11 years on average, solar thermal panels appear to be less costly than solar PV systems. Hakimi et al. [43] carried out a thermo-economic analysis to compare the performance of a PV, Central Tower Receiver (CTR) plant, and a Parabolic Trough Collector (PTC) plant with and without storage for the Herat, AFG. Through the Typical Meteorological Year (TMY) data generated by Meteonorm software, this analysis shows that the PTC plant with energy storage has the highest efficiency of about 43 % which is approximately 50 % more than the PV plant but the PV plant has more uniform power production profile. PTC with energy storage displays 25 % more power output than PTC



without energy storage. The Leveled Cost of Electricity is 0.146 \$/kWh for the CTR plant, 0.063 \$/kWh for the PV plant, 0.1076 \$/kWh for the PTC plant with energy storage, and 0.104 \$/kWh for the PTC plant without storage.

### **6.3.2 Solar light- gathering**

The most basic method of SE utilization is light-gathering. The solar radiation is converged by a mirrored surface with high specular reflection to provide concentrated light from the sun into the receiving surface. A solar cooker is a device that uses solar radiation to cook and heat food, which is a good example of light-gathering utilization [44]. The rural population of AFG is almost entirely reliant on biomass fuels for cooking and heating, resulting in air pollution. More than two-thirds of the population lives in rural areas, where traditional fuels are used and power is scarce. As a result, light-gathering can be used effectively in a wide range of building applications in AFG's rural areas.

### **6.3.3 Solar photovoltaic**

Photovoltaic is the most convenient way to use SE by converting it directly into electricity. Solar power is typically produced in a building using concentrating photovoltaic (CPV) systems and conventional flat-panel devices. CPV systems have many advantages over traditional flat-panel devices in buildings [8]. These systems, in comparison to conventional flat modules, allow for a more compact use of space, with facades and roofs in buildings, which are the program's target areas [45]. Furthermore, CPV aims to reduce the cost of PV by using less expensive concentrator materials rather than expensive solar cell materials [46]. In AFG, the energy sector is one of the least developed, with nearly 70 % of the country's population lacking access to electricity [32]. Energy has always been one of the most basic human needs, and now it is one of the Afghan people's most pressing and fundamental issues. Even in large cities of AFG, the government has not been able to take sufficient steps to address or reduce the issue of electricity. Therefore, CPV systems are a viable option for addressing AFG's electricity shortage.

## **7. Discussion**

There is a big chance for SE integration in AFG's building sector. The country's abundant solar resources and rapidly increasing energy consumption strengthen the argument for utilizing SE to address the country's energy issues. Despite the immense potential, successful implementation requires careful consideration of a few factors.

The Table 1. provides an overview of the critical points discussed regarding SE utilization in Afghan buildings, highlighting energy consumption patterns, solar potential, and the effectiveness of different solar technologies. A building's attributes largely determine its SE potential. The analysis of urban morphology and building orientation highlights the importance of optimizing building design for SE capture. The domed roofs of traditional Afghan architecture make for an intriguing case study when examining the possibilities of atypical building forms for SE collection. More investigation is necessary to calculate the energy savings from such architectural features.

Table 1. Energy consumption patterns, solar potential, and the effectiveness of solar technologies

Parameter	Value/Insight
Energy Consumption in Buildings (AFG Residential)	54 % of total energy consumption in AFG; annual consumption ranges from 178 kWh/household (Ghor) to 3,000 kWh/household (Kabul)
Average Solar Potential (GHI)	6.5 kWh/m <sup>2</sup> /day
Solar Radiation Hours	Over 3,000 hours of sunshine annually; more than 300 sunny days per year
Estimated SE Production	220 gigawatts
Government Target for RE	5,000 MW by 2032 (95 % of national electricity demand)
Solar Assets (Global Solar Intensity)	1370 W/m <sup>2</sup> outside of Earth's atmosphere; high solar radiation with an average of 6.5 kWh/m <sup>2</sup> /day
Urban Morphology's Impact on SE	Ceilings and facades can increase solar radiation capture by 9 % to 45 % based on optimal morphology; reductions in SE due to dense urban environments
Solar Radiation on Domed Roofs	Domed roofs receive more solar radiation compared to flat roofs.
Flat Roof Solar Potential	Maximum annual radiation: 4717.72 MJ/m <sup>2</sup> ; Minimum annual radiation: 342.58 MJ/m <sup>2</sup>
Solar Thermal Technologies in Buildings	Efficient for heating, cooling, and power generation; PTC plants with energy storage have 43 % efficiency and a leveled cost of \$0.1076/kWh
Solar Light-Gathering in Rural Areas	Effective for rural cooking/heating needs, especially in areas lacking access to electricity
CPV Systems for Electricity in Buildings	Suitable for addressing AFG's electricity shortage; compact for urban rooftops and facades; cost-effective alternative to traditional PV systems

AFG's diverse climate presents both challenges and opportunities for SE utilization. While the country experiences high solar radiation during the summer months, the winter months can be characterized by lower solar irradiance and increased cloud cover. To mitigate these seasonal variations, it is important to optimize the design and operation of SE systems. For instance, high-efficiency solar panels and advanced inverter technologies can help maximize energy output during periods of low solar radiation. Additionally, incorporating energy storage solutions, such as batteries or thermal storage, can help ensure a reliable and consistent power supply. Selecting the right SE technology is essential for maximizing production and lowering expenses. Although solar thermal systems are more economical, concentrated solar power (CSP) technologies have the potential to produce energy with greater yields. PV systems can offer a hybrid solution to satisfy various energy needs, especially when combined with CSP. Technical improvements and economic factors will influence the best technology option for various building types and locations in AFG.

To fully realize the potential of SE in AFG's building sector, a supportive policy and regulatory framework is important. Implementing feed-in tariffs, tax incentives, and accelerated depreciation can encourage private investment and reduce upfront costs for solar installations. Streamlining permitting procedures and providing technical assistance can facilitate the integration of SE into buildings. Additionally, long-term support for research and development is essential to improve the efficiency and reduce the cost of solar technologies. By adopting these policy measures, AFG can create a conducive environment for SE adoption and accelerate the transition to a sustainable energy future.

Even though this study offers insightful information about the potential of SE in AFG's building industry, more investigation is required to fully address certain opportunities and challenges. It is imperative to do a thorough examination of the financial viability of various SE solutions, taking into account variables like installation charges, ongoing maintenance costs, and energy conservation. Investigating the integration of energy storage devices to overcome the intermittent nature of solar power would also enhance the dependability and value proposition of SE solutions.

## **8. Conclusion**

AFG's abundant solar resources offer a significant opportunity to alleviate the country's chronic energy shortages, particularly in the building sector. However, the energy sector faces considerable challenges due to security concerns, infrastructure limitations, and a lack of widespread adoption of RE technologies.

The evaluation of solar radiation across various cities in AFG, as shown in Table 2, identifies Herat as the most promising location for SE exploitation. Herat exhibits the highest summer peak radiation at 8.7 kWh/m<sup>2</sup>/day and stable winter levels at 4 kWh/m<sup>2</sup>/day, ensuring consistent year-round energy generation. Kandahar, Farah, and Hilmand also show strong potential, with summer peaks of 8.5 kWh/m<sup>2</sup>/day and winter levels around 4.0 kWh/m<sup>2</sup>/day, making them suitable for sustainable energy projects. Nangarhar and Zabul demonstrate good solar potential, with summer peaks of 8.0 kWh/m<sup>2</sup>/day and steady winter values of 4.0 kWh/m<sup>2</sup>/day. In contrast, Balkh, Kabul, Ghazni, Urozgan, and Nimroz exhibit moderate suitability due to slightly lower radiation values, with winter radiation levels ranging between 3.0 and 3.5 kWh/m<sup>2</sup>/day. Paktika, with the lowest radiation levels (6.5 kWh/m<sup>2</sup>/day in summer and 3.1 kWh/m<sup>2</sup>/day in winter), is the least favorable location for SE development. These findings highlight the need to prioritize southwestern and western regions with higher solar radiation levels to maximize the efficiency and sustainability of SE systems in AFG. Additionally, climatic and geometrical factors play a crucial role in optimizing SE capture for buildings. By leveraging solar energy, AFG can move toward a more sustainable and energy-independent future.

Integrating SE into building energy systems is essential for AFG's sustainable development. This study emphasizes three forms of SE utilization in buildings, focusing on their functionalities and cost-effectiveness:

- Solar concentrators with thermal performance can reach higher temperatures and are therefore suitable for use in building heating.
- CPV can generate electric energy for buildings while saving PV materials and costs.
- For AFG's rural areas, solar light-gathering can provide more convenient and clean cooking and heating systems.

The findings of this study are relevant to other countries in Central Asia and the Middle East, such as Uzbekistan, Tajikistan, Kazakhstan, Iran, Iraq, Egypt, and Morocco, which share similar geographical, climatic, and socioeconomic conditions. For instance, Uzbekistan, with its arid climate and high solar radiation, faces similar challenges in grid infrastructure and energy security as AFG. By learning from AFG's experiences in SE deployment, Uzbekistan can accelerate its transition to a sustainable energy future. Similarly, countries like Egypt and Morocco, with their ambitious RE targets, can benefit from AFG's insights into policy frameworks and regulatory incentives.

Table 2. Comparative Solar Radiation Evaluation for Cities

City	Summer Peak Radiation (kWh/m <sup>2</sup> /day)	Winter Radiation (kWh/m <sup>2</sup> /day)	Year-Round Suitability
Herat	8.7	4	Excellent
Kandahar	8.5	4.3	Excellent
Farah	8.5	4.1	Excellent
Hilmand	8.5	4.2	Excellent
Nangarhar	8	4	Very Good
Zabul	8	4	Very Good
Balkh	7.5	3.5	Good
Kabul	7.5	3	Good
Ghazni	7	3	Moderate
Urozgan	7	3	Moderate
Nimroz	8	3.5	Moderate
Paktika	6.5	3.1	Low

## Abbreviations

AFG	Afghanistan
CPV	Concentrating Photovoltaic
CSP	Concentrating Solar Power
CTR	Central Tower Receiver
DNI	Direct Normal Irradiance
GHG	Greenhouse Gas
GHI	Global Horizontal Irradiance
GWh	Giga Watt Hour
kWh	Kilowatt-hour
LPG	liquefied petroleum gas
NREL	National Renewable Energy Laboratory of the US
PTC	Parabolic Trough Collector
PV	Photovoltaic
R	Pearson correlation coefficient
R <sup>2</sup>	Squared Pearson Correlation Coefficient
RE	Renewable Energy
SE	Solar Energy
SVF	Sky View Factor
TMY	Typical Meteorological Year

## Author Contribution

Edris Naseri: Conceptualization, Methodology, Investigation, Writing and Editing  
 Burcin Deda Altan: Methodology, Review & Editing  
 Afsin Gungor: Conceptualization, Review & Editing

## References

- [1] Shroder, J.F., Natural resources in Afghanistan: geographic and geologic perspectives on centuries of conflict. Elsevier, 2014.

- [2] Nations, U., Department of economic and social affairs population dynamics. World Urbanization Prospects, 2018.
- [3] Organization, W.H., WHO guidelines for indoor air quality: household fuel combustion. World Health Organization, 2014.
- [4] Pearce, J.M., Photovoltaics—a path to sustainable futures. *Futures*, 34(7), 663-674, 2002.
- [5] Zhong, X., et al., The evolution and future perspectives of energy intensity in the global building sector 1971-2060. *Journal of Cleaner Production*, 305, 127098, 2021.
- [6] Cao, X., X. Dai, and J. Liu, Building energy-consumption status worldwide and the state-of-the-art technologies for zero-energy buildings during the past decade. *Energy and buildings*, 128, 198-213, 2016.
- [7] Ouria, M. and H. Sevinc, Evaluation of the potential of solar energy utilization in Famagusta, Cyprus. *Sustainable cities and society*, 37, 189-202, 2018.
- [8] Aldegheri, F., et al., Building integrated low concentration solar system for a self-sustainable Mediterranean villa: The Astonysine house. *Energy and buildings*, 77, 355-363, 2014.
- [9] Ludin, G.A., et al., Technical and economic analysis of an HVDC transmission system for renewable energy connection in Afghanistan. *Sustainability*, 14(3), 1468, 2022.
- [10] Amarkhail, S., Potential and utilization of renewable energy sources in Afghanistan. *Journal of Engineering Research and Applied Science*, 11(1), 2032-2038, 2022.
- [11] Jahangiri, M., et al., Investigating the current state of solar energy use in countries with strong radiation potential in asia using GIS software, a review. *Journal of Solar Energy Research*, 5(3), 477-497, 2020.
- [12] Shukla, A.K., K. Sudhakar, and P. Baredar, Renewable energy resources in South Asian countries: Challenges, policy and recommendations. *Resource-Efficient Technologies*, 3(3), 342-346, 2017.
- [13] Milbrandt, A. and R. Overend, Assessment of biomass resources in Afghanistan. National Renewable Energy Lab.(NREL), Golden, CO (United States), 2011.
- [14] Pulsipher, L.M., et al., World regional geography: global patterns, local lives, New York, NY: W.H. Freeman and Company; 7th edition 2017.
- [15] Shroder, J.F. and S.J. Ahmadzai, Transboundary water resources in Afghanistan: Climate change and land-use implications, Elsevier 2016.
- [16] Palka, E.J., Afghanistan: A Regional Geography. 2001.
- [17] Burns, R.K., Afghanistan: Solar assets, electricity production, and rural energy factors. *Renewable and Sustainable Energy Reviews*, 15(4), 2144-2148, 2011.
- [18] Cozzi, L., et al. World Energy Outlook. IEA Paris, 2020.
- [19] Bose, B.K. Energy, environment, and advances in power electronics. in ISIE'2000. Proceedings of the 2000 *IEEE International Symposium on Industrial Electronics*. IEEE, 2000.
- [20] Kober, T., et al., Global energy perspectives to 2060—WEC's World Energy Scenarios 2019. *Energy Strategy Reviews*, 31, 100523, 2020.
- [21] Conti, J.J., et al., Annual energy outlook 2014. US Energy Information Administration, 2014.

- [22] Bank, W., Energy Security Trade-Offs Under High Uncertainty: Resolving Afghanistan's Power Sector Development Dilemma. World Bank, 2016.
- [23] Aminjonov, F., Afghanistan's energy security. *Tracing Central Asian countries' contribution*, 1-30, 2016.
- [24] Ershad, A.M., R.J. Brecha, and K. Hallinan, Analysis of solar photovoltaic and wind power potential in Afghanistan. *Renewable Energy*, 85, 445-453, 2016.
- [25] Ahmadzai, S. and A. McKinna, Afghanistan electrical energy and trans-boundary water systems analyses: Challenges and opportunities. *Energy Reports*, 4, 435-469, 2018.
- [26] Mohammad, A., P. Shrestha, and S. Kumar, Urban residential energy use in Kandahar, Afghanistan. *Cities*, 32, 135-142, 2013.
- [27] Nejat, P., et al., A global review of energy consumption, CO2 emissions and policy in the residential sector (with an overview of the top ten CO2 emitting countries). *Renewable and sustainable energy reviews*, 43, 843-862, 2015.
- [28] Korkovelos, A., et al., A GIS approach to planning electrification in Afghanistan, 2017.
- [29] Martins, F.R., et al., Data generated by evaluating the seasonal variability and trend analysis of the solar energy resource in the Northeastern Brazilian region. *Data in brief*, 26, 104529, 2019.
- [30] Sayigh, A., Solar energy application in buildings. *Elsevier*, 2012.
- [31] Mohmand, R. and A. Mohan, Potential of Solar Energy in Afghanistan. *Journal of Critical Reviews*, 7(12), 2644-2652, 2020.
- [32] Safi, R. and M. Sharma, Energy Scenario of Afghanistan. *Energy*, 9(4), 2019.
- [33] Renné, D.S., et al. Solar and wind resource assessments for Afghanistan and Pakistan. *Proceedings of ISES World Congress 2007* (Vol. I–Vol. V). Springer, 2008.
- [34] Anwarzai, M.A. and K. Nagasaka, Utility-scale implementable potential of wind and solar energies for Afghanistan using GIS multi-criteria decision analysis. *Renewable and Sustainable Energy Reviews*, 71, 150-160, 2017.
- [35] Faghih, A.K. and M.N. Bahadori, Solar radiation on domed roofs. *Energy and Buildings*, 41(11), 1238-1245, 2009.
- [36] Çalışkan, O. and S. Marshall, Urban Morphology and Design Introduction, 2011.
- [37] Sarralde, J.J., et al., Solar energy and urban morphology: Scenarios for increasing the renewable energy potential of neighbourhoods in London. *Renewable Energy*, 73, 10-17, 2015.
- [38] Poon, K.H., et al., Parametric study of URBAN morphology on building solar energy potential in Singapore context. *Urban Climate*, 33, 100624, 2020.
- [39] Li, Y., et al., A pixel-based approach to estimation of solar energy potential on building roofs. *Energy and Buildings*, 129, 563-573, 2016.
- [40] Kanters, J. and M. Horvat, Solar energy as a design parameter in urban planning. *Energy Procedia*, 30, 1143-1152, 2012.
- [41] Yang, L., B.-j. He, and M. Ye, The application of solar technologies in building energy efficiency: BISE design in solar-powered residential buildings. *Technology in Society*, 38, 111-118, 2014.
- [42] Blanco, M. and L.R. Santigosa, Advances in concentrating solar thermal research and technology. Woodhead Publishing, 1st edition, 2016.

- [43] Hakimi, M., E. Baniasadi, and E. Afshari, Thermo-economic analysis of photovoltaic, central tower receiver and parabolic trough power plants for Herat city in Afghanistan. *Renewable Energy*, 150, 840-853, 2020.
- [44] Ahmed, S.M., et al., Design, construction and testing of parabolic solar cooker for rural households and refugee camp. *Solar Energy*, 205, 230-240, 2020.
- [45] Marín-Sáez, J., et al., Outdoor performance evaluation of a holographic solar concentrator optimized for building integration. *Applied Energy*, 250, 1073-1084, 2019.
- [46] Sellami, N. and T.K. Mallick., Design of nonimaging static solar concentrator for window integrated photovoltaic. *AIP Conference Proceedings*. American Institute of Physics, 2012.
- [47] Global Solar Atlas. <https://globalsolaratlas.info/global-pv-potential-study>. Accessed 15 April 2024.



## Assessment of Concrete Pavement Performance on Istanbul's BRT Lines

Aydın Kıcı

Suleyman Demirel University, Faculty of Engineering and Natural Sciences, Department of Civil Engineering,  
Isparta, Turkey

✉: [aydinkici@yahoo.com](mailto:aydinkici@yahoo.com) : 0000-0001-9741-4995

Received: 14.11.2024, Revised: 12.12.2024, Accepted: 16.12.2024

### Abstract

The performance of concrete pavements is directly related to stresses and vertical displacements generated by vehicle loads. Selecting appropriate pavement and base thickness is crucial for extending service life in heavy vehicle areas like Istanbul's bus rapid transit lines. This study aims to calculate the maximum stress and vertical displacements caused by Istanbul's bus rapid transit vehicles on concrete pavements. There are currently four types of buses actively operating on Istanbul's bus rapid transit line, each with different axle configurations and load capacities. Stresses and vertical displacements were calculated for the heaviest axle configuration of these buses under edge and center loading conditions using the Finite Element Method (FEM). These analyses were repeated across three different overlay conditions: concrete overlay of asphalt, concrete overlay of concrete, and concrete overlay on granular base. A total of 24 analyses, covering various loading conditions and pavement configurations, were conducted using the EverFE software. This research reveals maximum stress and vertical displacement values under various loading conditions, base properties, and slab thicknesses, offering critical insights for determining pavement thickness and guiding maintenance strategies. This study also fills the gap in the literature regarding the determination of concrete pavement thickness for BRT lines.

**Keywords:** Bus rapid transit (BRT), concrete pavement, structural design, FEM, foundation materials.

### 1. Introduction

Concrete pavements offer significant advantages in carrying traffic loads on roads exposed to heavy vehicle traffic, with their low-cost and environmentally friendly characteristics [1-3]. Thanks to their high bearing capacity and rigidity, concrete pavements can effectively distribute traffic loads over broader and more uniform areas to the base and subbase layers, making them an effective alternative to asphalt concrete pavements in numerous road applications [4-6].

At first, concrete slab thickness was determined exclusively by experimental research and observation. However, with the advancement of numerical and FE methods, it has become possible to examine the structural responses of slabs [7]. Westergard, who is considered a pioneer of these studies, developed closed-form formulas using FEM to calculate maximum strains and maximum displacements [8]. After these studies, the structural response of concrete pavements under vehicle loads became the main method for thickness design. In the thickness design of concrete pavements, two criteria "erosion" and "fatigue" began to be taken into consideration [8-11]. The PCA 1984 method is one of the primary mechanical methods developed by considering stresses and vertical displacements. The two damage conditions identified by this procedure are erosion and fatigue. The fatigue damage of the concrete pavement is determined by maximum strain, and the erosion damage of the base layer is determined by vertical displacements [12].





There are three primary types of concrete pavements used in road projects: continuously reinforced concrete pavement (CRCP), jointed reinforced concrete pavement (JRCP), and jointed plain concrete pavement (JPCP). Although concrete slabs are designed in different types, two main properties are expected from all of them. The first of these is to exhibit good performance against axle loads on the pavement structure by utilizing the flexural strength of concrete, ensuring that the bending stresses remain below this flexural strength. The second is to resist shrinkage tendencies of the concrete due to the release of hydration energy during the setting process, along with expansion tendencies induced by environmental factors [3,13].

Today, in addition to traditional concrete pavements, roller compacted concrete pavements (RCCP) and concrete pavements constructed with a slipform paver, which are produced using specially prepared gradations, have also become widely used in road construction. These type of pavement can be swiftly placed and compacted, and in a matter of days, it can be made accessible to traffic. These characteristics make them ideal for roads that need to be opened to traffic urgently. Additionally, they offer long-lasting performance with their durable structure and require minimal maintenance especially under heavy traffic conditions [14,15].

In the literature, there are some studies that examine the mechanical effects caused by vehicle loads on asphalt and concrete pavements using FEM. In their study, Singh and Ghosh analyzed the mechanical stresses occurring in concrete pavements under vehicle axle loads and environmental loads using the SAP2000 FEM software [16]. The performance of BRT lines in Nevada, USA, under high bus loads was investigated by Hajj et al. The Nevada BRT line used asphalt pavements, so their study included rutting and fatigue analyses [17]. In his study, Vargas analyzed the transitions between Portland Cement Concrete Pavements (PCCP) and Asphalt Concrete Pavements (ACP) constructed for Bogotá's BRT lines, TransMilenio, using the Abaqus FEM software. He examined the dynamic loading effects caused by vehicles at the concrete-asphalt pavement transitions [18].

There are numerous studies focused on enhancing the mechanical and strength properties of concrete and soils by adding fibers [19-22]. Concrete is transformed into a composite material by adding fibers. The primary purpose of these fibers is to improve crack control by increasing the concrete's flexural and tensile strength. Adding fibers to concrete used as road pavement will increase its resistance to tensile stresses on the top and bottom surfaces of the concrete due to repeated axle loads and environmental conditions. In addition to improving the pavement's fatigue and erosion performance, this will increase its resistance to cracking [23-25]. Although fibers additives to concrete improve flexural strength and crack resistance, they do not have a significant effect on compressive strength or static modulus of elasticity [26, 27]. Its effect on Poisson's ratio is also quite limited. Therefore, the stresses occurring in concrete pavements under vehicle loads are not highly related to whether the concrete contains fibers or not.

Concrete pavements can be constructed directly on natural or granular subgrades. Nonetheless, they may be constructed on top of pre-existing pavements. In this regard, concrete pavements can be constructed in a composite structure as concrete overlay of asphalt and concrete overlay of concrete [28]. In the Istanbul BRT network, known as the 'Metrobus' system, concrete pavement applications have started to involve both concrete overlays of asphalt and concrete overlays of concrete [29]. In this context, a total of 35.9 km (71.8 km for the round trip) of roads were covered with concrete pavement, commonly referred to as 'white road' by Istanbul Municipality, in three stages, starting from 2022 [30].

In this paper, stress and vertical displacements were calculated caused by Istanbul's BRT transit vehicles through FEM analysis. The four types of buses currently operating on the Istanbul BRT line are the Mercedes Conecto, Mercedes Capacity, Otokar Kent XL, and AKIA Ultra

LF25. The heaviest axle loads of these four vehicles have been selected as critical axle loads and used in the analyses. The analyses were repeated for three different overlay conditions: concrete overlay of asphalt, concrete overlay of concrete, and concrete overlay on granular base, with the first two already in use at the Istanbul BRT line. Using the EverFE FEM software, a total of 24 evaluations covering different pavement layouts and loading situations were carried out. There are limited studies in the literature that investigate the stress and vertical displacements caused by BRT lines and the vehicles operating on these lines. This study has unique value in filling this gap in literature. Additionally, the study examines stress and deformations under three different pavement conditions on the same BRT line represents another distinctive aspect of the work.

## 2. Material and Method

Istanbul's BRT service, which began with an 18.3 km line in September 2007, has expanded to become the city's most important transit system, with a 52 km one-way total length and 44 stations [30]. The primary public transit system in the city, Istanbul BRT connects to numerous other forms of transportation. From the beginning, the Istanbul BRT line has been run on an asphalt surface. However, under the intense repetitive traffic of heavy vehicles on the BRT line, it has suffered from various deteriorations, primarily including ruttings (Fig. 1.). Because of the BRT lane's narrowness, the tires of the vehicles travel on a single track, accelerating the development of rutting. After experiences with the low serviceability and high maintenance costs of the asphalt on the BRT line, the Istanbul Municipality adopted a concrete road application through a three-phase program.



Fig. 1. Asphalt deterioration in Istanbul BRT line [31]

BRT buses' sizes and high axle loads are the main factors behind the Istanbul municipality's wish to convert to concrete roads. The vehicles currently in use, including the Mercedes Conecto, Mercedes Capacity, Otokar Kent XL, and AKIA Ultra LF25, are high-capacity buses specifically designed for these roads. The number of BRT vehicles in the inventory of the Istanbul Municipality and their associated characteristics are as shown in Table 1.

In this study, the stresses and vertical displacements occurring on concrete pavements are examined based on the heaviest axle weight of each bus. As a result, the vehicles' axle construction and size have also been taken into account. The sizes of these vehicles range from 18 to 25 meters. The number of axles ranges from 3 to 5 and the axle configurations and spacing of the axles of these vehicles are presented in Fig. 2.

Table 1. Istanbul BRT vehicle details

	Mercedes Conecto G [32]	Mercedes Capacity [33]	Otokar Kent XL [34]	Akia Ultra LF 12 [35]
Vehicle length (mm)	18124	19725	20995	25000
Vehicle width (mm)	2550	2550	2540	2550
Axle spacings (mm)	1 <sup>st</sup> -2 <sup>nd</sup> 5900 2 <sup>nd</sup> -3 <sup>rd</sup> 5990	1 <sup>st</sup> -2 <sup>nd</sup> 5900 2 <sup>nd</sup> -3 <sup>rd</sup> 5990 3 <sup>rd</sup> -4 <sup>th</sup> 1600	1 <sup>st</sup> -2 <sup>nd</sup> 5900 2 <sup>nd</sup> -3 <sup>rd</sup> 7385 3 <sup>rd</sup> -4 <sup>th</sup> 1600	1 <sup>st</sup> -2 <sup>nd</sup> 5868 2 <sup>nd</sup> -3 <sup>rd</sup> 6652 3 <sup>rd</sup> -4 <sup>th</sup> 6680 4 <sup>th</sup> -5 <sup>th</sup> 2790
Maximum axle load (kg)	13200	13000	11500	12000
Gross weight (kg)	30500	32000	34000	45000
Seats	40	44	39	29
Standing capacity	110	137	182	252
Total capacity	150	181	221	281

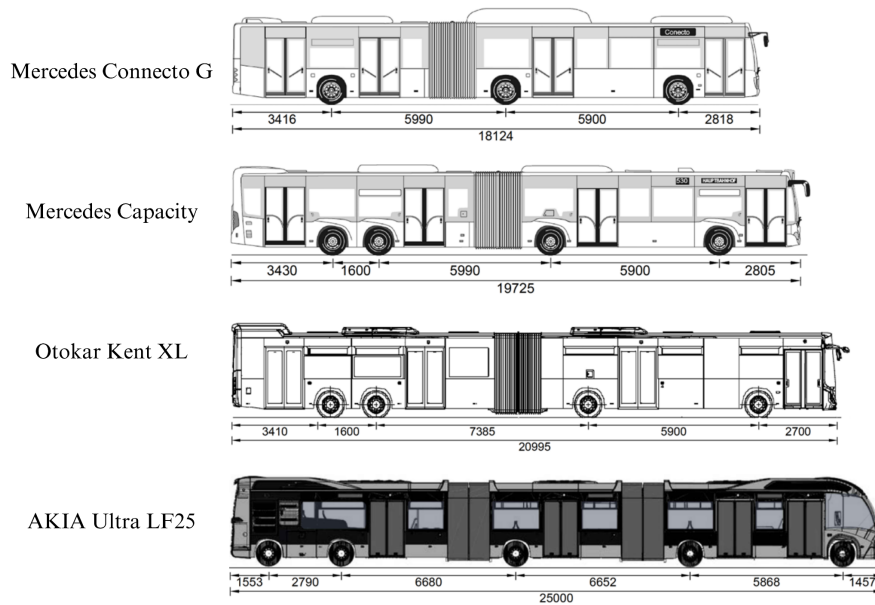


Fig. 2. Vehicle on the Istanbul BRT Line [32-35]

Considering the heavy usage and critical importance of the Istanbul BRT line, the Istanbul Municipality has chosen concrete road technology that can be laid with a slip-form paver to accelerate construction processes. The existing concrete and asphalt pavements were also chosen to serve as a base layer throughout the building phase. According to the technical specifications from the tender documents, two different layer structures were applied: concrete overlay of asphalt and concrete overlay of concrete [29]. It is thought that the concrete pavement was constructed directly on top of the granular subgrade in some sections. Consequently, it is noted that different BRT line segments utilize various layer structures. The pavement thicknesses of the three different layer structures are shown in Fig. 3. In Table 1, the selected material properties used in the pavement layer analysis are presented. The table includes the modulus of elasticity and Poisson's ratios for the newly placed fiber-reinforced C40 concrete, C25 existing concrete, existing asphalt pavement, and granular base layer. These parameters were chosen to represent each material's specific mechanical characteristics in the analysis.

The pavement width of 330 cm was selected as part of the three-phase concrete pavement transition project for the Istanbul BRT line. Joint applications were positioned every 110 cm throughout this width, which was split horizontally into three equal sections. Longitudinally, joints were also placed at intervals of 110 cm, creating 110x110 cm square sections. In the construction method, a slipform concrete paver was used, and high-quality (C40) concrete with polypropylene/polyamide fiber reinforcement was utilized. In Table 2, the estimated material and layer properties are presented.

Table 2. Material Properties for Layers

Material	Modulus of elasticity (GPa)	Poisson's ratio	Density (kg/m <sup>3</sup> )
Fiber-Reinforced Polypropylene Concrete Pavement (C40)	34.0	0.15	2300
Existing Concrete (C25)	30.0	0.15	2300
Existing Asphalt Pavement	1.0	0.30	2300
Granular Base Layer	0.3	0.25	2200

The axle weights of four vehicles actively serving on the Istanbul BRT line were examined. Analyses have been conducted based on the axles that, in terms of stresses and vertical displacements, put the most impact on the pavement. The following four axle configurations were selected for analysis: the third axle (rear) weighing 13.2 tons for the Mercedes Conecto G model, the third axle with a weight of 13 tons for the Mercedes Capacity model, the third axle weighing 11.5 tons for the Otokar Kent XL, and both the second and third axles, each weighing 12 tons, for the Akia Ultra LF25.

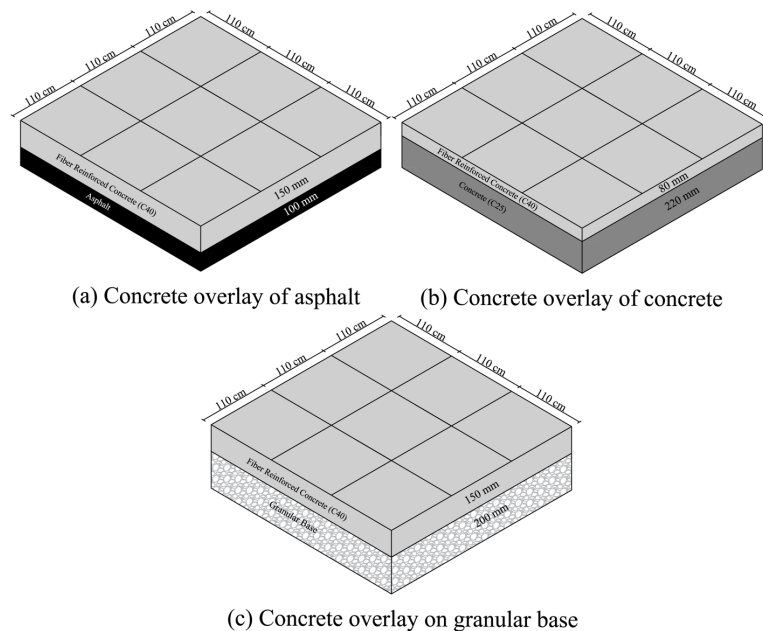


Fig. 3. Layers of the analyzed pavements

A detailed analysis of the selected axles revealed dual wheel configuration at both ends, with a wheel size of 275/70 R 22.5 used in the study. The axle structure corresponding to the applied loadings is illustrated in Fig. 4.

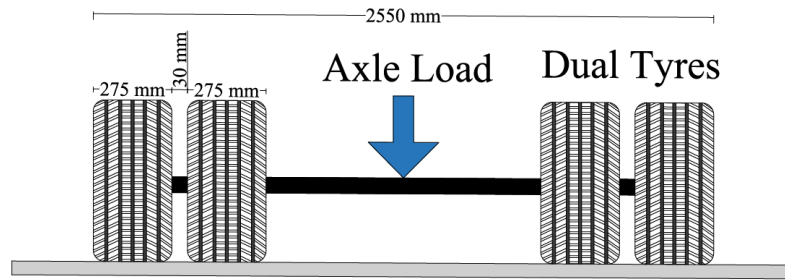


Fig. 4. Critical axle configuration of buses

Given that Istanbul BRT lanes are only 3300 mm wide and vehicle widths are 2550 mm, it can be concluded that most vehicles follow the same route. Therefore, for each selected axle load, it is assumed that the axles are centered within their lane, and two different loading positions, at the center and edge of the slab, have been specified. Six different combinations have been identified based on two loading positions (L1 - mid-slab, L2 - edge) and three types of pavement base and thickness (BT1 - concrete overlay of asphalt, BT2 - concrete overlay of concrete, and BT3 - concrete overlay on granular base) (Fig. 5). For these six selected combinations, repeated analyses were conducted using axle weights from four different buses, resulting in a total of 24 analyses.

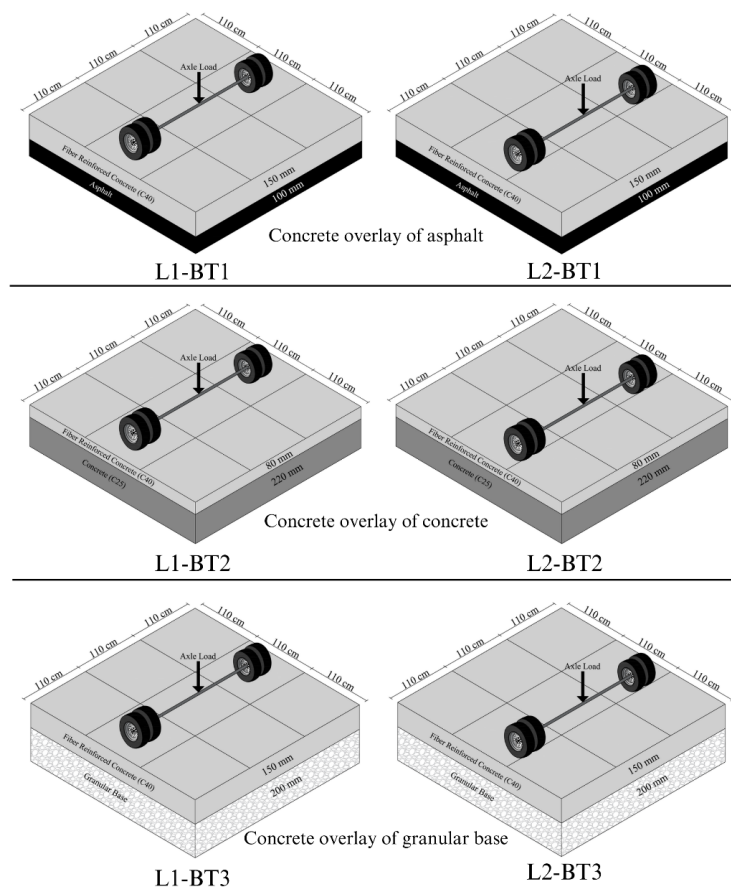


Fig. 5. Loading position and pavement structure combinations

In this study, 24 different finite element analyses are classified with codes assigned to each loading scenario. For the loading combinations, four different axle loads (A1, A2, A3, A4), two different loading conditions (L1, L2), and three different pavement types (BT1, BT2, BT3)

were used. Table 3. provides a systematic overview of each code combination, along with the associated loading condition and pavement type, to support the organized tracking of all scenarios utilized in the analyses. This coding system was developed to simplify the examination of the effects of different loading and pavement parameters on the results.

Table 3. Loading and pavement codes of scenarios

<b>Critical axle loads</b>	
A1	Mercedes Conecto G - Rear Axle - 13.2 tons
A2	Mercedes Capacity - 3th Axle - 13.0 tons
A3	Otokar Kent XL - 3th Axle - 11.5 tons
A4	AKIA Ultra LF25 - 3th 4th Axle - 12.0 tones
<b>Loading positions</b>	
L1	Mid-slab loading
L2	Edge loading
<b>Base and Thickness</b>	
BT1	Concrete overlay (150 mm) of asphalt (100 mm)
BT2	Concrete overlay (80 mm) of concrete (200 mm)
BT3	Concrete overlay (150 mm) on granular base (200 mm)

The FEM has been developed as a powerful tool for the numerical solution of many problems, especially in engineering, and its applications are increasingly widespread. It has been used in numerous studies on concrete pavements to address vehicle loads and environmental factors. Today, the FEM can be applied using various software. For concrete pavement analysis, there are general-purpose finite element software options such as Ansys and Abaqus, as well as programs specifically designed for concrete roads, including EverFE, ISLAB, and KENSLABS. The EverFE [36-41] software, which is frequently used by researchers, was employed in this study. This methodology provides a significant advantage by enabling detailed modeling of the stress and deformation behavior of concrete pavements under axle and environmental loadings, thereby offering a reliable approach to optimizing pavement design and maintenance strategies.

### 3. Results and Discussions

Numerical analyses were completed using the EverFe software under various loading and layer conditions, and the stresses and vertical displacements were calculated. For this, the thicknesses and material properties of the layers were initially defined in the software. Then, the thicknesses and material characteristics of the pavement layers were specified, and the interface condition between the base and pavement was set as bonded. The axle loads and configurations of the vehicles were determined. Finally, the meshing process was completed before performing the analysis. Images of some selected analyses for performed in the EverFe program, showing the stress distribution underneath the pavement, are presented in Fig. 6.



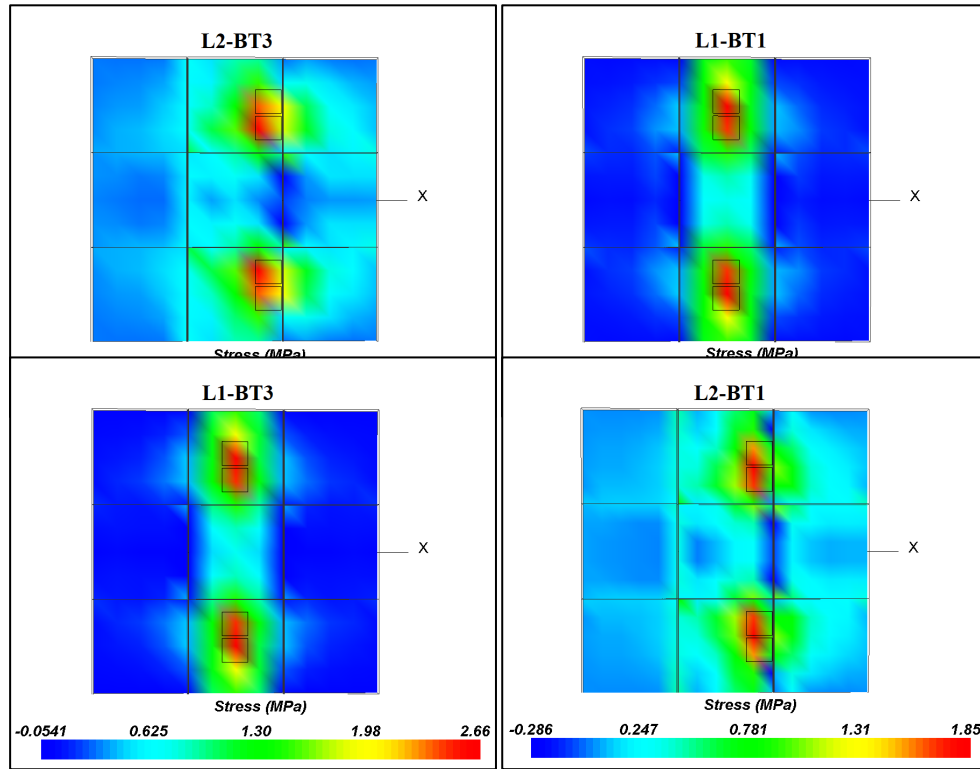


Fig. 6. Stress distribution of A1 axle loading in selected analyses

The analysis in this study shows that the Istanbul BRT vehicles generate significant stress and vertical displacement in concrete pavements. The effect of different base layers and concrete pavement thicknesses on stress and vertical displacement is investigated in this study. The maximum principal stress, maximum flexural stress, and maximum displacement values for the 24 scenarios examined in the study are presented in Table 4. In line with findings from previous studies [42, 43], the most critical stress region for concrete pavements is the stress that occurs at the interface between the pavement and the underlying base, that is, at the bottom surface of the pavement. Therefore, when determining the stresses, the section of the bottom surface of the pavement was considered, and the stress values in that area were presented.

As a result of the analyses, the highest stress among the examined conditions was observed under the 13.2-ton axle load of the Mercedes Conecto G model, with mid-slab pavement loading, in the case where granular base was used (A1-L1-BT3), with a maximum stress of 2.66 MPa. The largest vertical displacement, 1.63 mm, was observed under the same load and layered structure condition, with edge loading (A1-L2-BT3).

Other axle loads were also examined, and the highest stresses occurred during mid-slab loadings, while the maximum vertical displacements were observed during edge loadings. For all loading conditions, the highest stress and vertical displacements occurred with the concrete overlay on granular base (BT3) base and thickness condition. Conversely, the lowest stresses and vertical displacements were observed in the case of the concrete overlay of concrete (BT2) base and thickness condition. These results indicate that the base layer has a significant impact on stresses and vertical displacements.

Table 4. Summary of stress and displacement results

Scenarios	Max displacement (mm)	Max principal stress (Mpa)	Max flexural stress(Mpa)	Scenarios	Max displacement (mm)	Max principal stress (Mpa)	Max flexural stress(Mpa)
A1-L1-BT1	1.10	2.54	2.54	A3-L1-BT1	0.98	2.21	2.21
A1-L1-BT2	0.71	0.26	0.14	A3-L1-BT2	0.65	0.23	0.13
A1-L1-BT3	1.17	2.66	2.66	A3-L1-BT3	1.05	2.32	2.32
A1-L2-BT1	1.60	1.85	1.76	A3-L2-BT1	1.42	1.61	1.54
A1-L2-BT2	0.83	0.36	0.16	A3-L2-BT2	0.75	0.31	0.14
A1-L2-BT3	1.63	1.66	1.41	A3-L2-BT3	1.45	1.45	1.23
A2-L1-BT1	1.09	2.23	2.22	A4-L1-BT1	1.02	2.31	2.31
A2-L1-BT2	0.71	0.26	0.15	A4-L1-BT2	0.67	0.24	0.13
A2-L1-BT3	1.16	2.62	2.62	A4-L1-BT3	1.09	2.42	2.42
A2-L2-BT1	1.58	1.82	1.74	A4-L2-BT1	1.47	1.68	1.60
A2-L2-BT2	0.82	0.35	0.16	A4-L2-BT2	0.78	0.32	0.14
A2-L2-BT3	1.61	1.45	1.23	A4-L2-BT3	1.50	1.51	1.29

Despite the thinness of the concrete pavement, loadings with a concrete base were observed to result in the lowest stresses and vertical displacements. The main reason for this is the high rigidity of the concrete used as the base. Among the examined conditions, the lowest pavement stress, 0.23 MPa, was observed under the 11.5-ton axle load of the Otokar Kent XL vehicle, with edge loading on the pavement, in the case where concrete was used as the base (A3-L1-BT2). The lowest displacement, 0.65 mm, was calculated in the A3-L1-BT2 scenario, where concrete was used as the base.

#### 4. Conclusions

This study thoroughly examined the maximum loads and displacements caused by Istanbul BRT vehicles' axles on concrete pavements in relation to pavement thickness and layer composition. The analyses utilized the actual axle loads of vehicles currently operating on the Istanbul BRT line, along with the pavement thicknesses and layer structures used in practice. Finite Element Method (FEM) analyses were conducted using the EverFe software to determine the maximum principal stress, flexural stress, and vertical displacements within the pavement. Some main conclusions may be drawn from the results, which are as follows:

- Among the examined conditions, the highest stress, 2.66 MPa, was observed under the 13.2-ton axle load of the Mercedes Conecto G model with mid-slab pavement loading and granular base (A1-L1-BT3), corresponding to approximately 33.3% of the estimated concrete flexural strength of 8 MPa.
- The largest vertical displacement, 1.63 mm, was noted under the same load and layered structure condition with edge loading (A1-L2-BT3).
- These findings contribute to the development of design and maintenance strategies tailored for heavy and high-traffic roadways. This study focused solely on stress and displacement assessments.
- Future studies may extend this work by examining the flexural stress-to-flexural strength ratio, along with fatigue and erosion analyses, using models such as PCA 1984.



- The insights from this research provide crucial information for determining appropriate pavement thickness by revealing maximum stress and vertical displacement values across various loading conditions, base properties, and slab thicknesses, thus supporting the advancement of effective maintenance strategies.

For future studies, assessing environmental impacts and evaluating the long-term performance of concrete pavements can improve the processes through field studies. The long-term performance of concrete pavements, combined with cost-benefit analyses, can form the basis of future research directions.

## References

- [1] Li, Z., Shen, A., Long, H., Guo, Y., He, T., Dynamic deterioration of strength, durability, and microstructure of pavement concrete under fatigue load. *Construction and Building Materials*, 306, 124912, 2021.
- [2] Leng, Z., Fan, Z., Liu, P., Kollmann, J., Oeser, M., Wang, D., Jiang, X., Texturing and evaluation of concrete pavement surface: A state-of-the-art review. *Journal of Road Engineering*, 252–265, 2023.
- [3] Delatte, N. J., *Concrete Pavement Design, Construction, and Performance*, Crc Press; 2<sup>nd</sup> edition, 2014.
- [4] Zhao, W., Zhang, J., Lai, J., Shi, X., Xu, Z., Skid resistance of cement concrete pavement in highway tunnel: a review. *Construction and Building Materials*, 406, 133235, 2023.
- [5] Huang, Y. H., *Pavement Analysis and Design*, Pearson Education Inc.; 2nd edition, 2004.
- [6] Jove, F., Millán, C., Burbano, J.L.A., Modeling of rigid pavements on clayey subgrades of low and medium plasticity in residential roads in Sincelejo City. *Journal of Positive Psychology and Wellbeing*, 7(1), 927-941, 2023.
- [7] Zdiri, M., Abriak, N., Neji, J., Ouezdou, M.B., Modelling of the stresses and strains distribution in an RCC pavement using the computer code "Abaqus". *Electronic Journal of Structural Engineering*, 9, 37-44, 2009.
- [8] Westergaard, H. M., Analysis of stresses in concrete pavement due to variations of temperature. *Proceedings, Highway Research Board*, 6, 201–215, 1926.
- [9] Kici, A., Tigdemir, M., A user friendly software for rigid pavement design. *International Journal of Engineering and Applied Sciences*, 9(4), 1-16, 2017.
- [10] Hernández López, F.M., Tejeda Piusseaut, E., Rodríguez Veliz, E.A., Recarey Morfa, C.A., 3D-FE of jointed plain concrete pavement over continuum elastic foundation to obtain the edge stress. *Revista de la construcción*, 19(1), 5-18, 2020.
- [11] Kici, A., Tiğdemir, M., Kalyoncuoğlu, Ş.F., Parametric study of the parameters affecting concrete pavement thickness. *Journal of the Institute of Science and Technology*, 8(3), 145-152, 2018.
- [12] Portland Cement Association (PCA), *Thickness Design for Concrete Highway and Street Pavements*, Engineering Bulletin EB109P. Skokie, IL: Portland Cement Association, USA, 1984.
- [13] Abadin, M.J., Kadir, A., Roy, S.K., Wei, Z.Z., Rahman, M.W., First experiences with continuously reinforced concrete pavement in national highway of Bangladesh. *International Journal of Pavement Research and Technology*, 1-28, 2023.

- [14] Selvam, M., Debbarma, S., Singh, S., Shi, X., Utilization of alternative aggregates for roller compacted concrete pavements–A state-of-the-art review. *Construction and Building Materials*, 317, 125838, 2022.
- [15] Debbarma, S., Ransinchung, G.D., Achieving sustainability in roller compacted concrete pavement mixes using reclaimed asphalt pavement aggregates–state of the art review. *Journal of Cleaner Production*, 287, 125078, 2021.
- [16] Singh, K., Ghosh, G., Stress behavior of concrete pavement. *Materials Today: Proceedings*, 55, 246-249, 2022.
- [17] Hajj, E.Y., Batioja-Alvarez, D., Siddharthan, R., Assessment of pavement damage from bus rapid transit: Case study for Nevada. *Transportation Research Record*, 2591(1), 70-79, 2016.
- [18] Vargas-Diaz, S.A., Finite Element Modeling of Direct Transition from Concrete Pavement to Asphalt Pavement. *TecnoLógicas*, 25(55), 2022.
- [19] Zhang, P., Wang, C., Gao, Z., Wang, F., A review on fracture properties of steel fiber reinforced concrete. *Journal of Building Engineering*, 67, 105975, 2023.
- [20] Yuhazri, M.Y., Zulfikar, A.J., Ginting, A., Fiber reinforced polymer composite as a strengthening of concrete structures: A review, *IOP Conference series: Materials science and engineering*, 1003, 1, 012135, IOP Publishing, 2020.
- [21] Yazıcı, M.F., Keskin, S.N., A Review on Soil Reinforcement Technology by Using Natural and Synthetic Fibers. *Erzincan University Journal of Science & Technology*, 14(2), 2021.
- [22] Yazıcı, M.F., Keskin, S.N., Experimental investigation of the mechanical properties of polypropylene fiber-reinforced clay soil and development of predictive models: effects of fiber length and fiber content. *Arabian Journal for Science and Engineering*, 1-19, 2024.
- [23] Altoubat, S.A., Roesler, J.R., Lange, D.A., Rieder, K.A., Simplified method for concrete pavement design with discrete structural fibers. *Construction and Building Materials*, 22(3), 384-393, 2008.
- [24] Geremew, A., De Winne, P., Demissie, T.A., De Backer, H., Treatment of natural fiber for application in concrete pavement. *Advances in Civil Engineering*, 2021(1), 6667965, 2021.
- [25] Kos, Ž., Kroviakov, S., Mishutin, A., Poltorapavlov, A., An experimental study on the properties of concrete and fiber-reinforced concrete in rigid pavements. *Materials* 16, 17:5886, 2023.
- [26] Del Savio, A.A., La Torre Esquivel, D., Carrillo, J., Chi Yep, E., Determination of polypropylene fiber-reinforced concrete compressive strength and elasticity modulus via ultrasonic pulse tests. *Applied Sciences*, 12(20), 10375, 2022.
- [27] Yağmur, E., Lifli betonlar için elastisite modülü tahmini. *Pamukkale Üniversitesi Mühendislik Bilimleri Dergisi*, 26(6), 1098-1109, 2020.
- [28] Vandenbossche, J.M., Dufalla, N., Li, Z., Bonded concrete overlay of asphalt mechanical-empirical design procedure. *International Journal of Pavement Engineering*, 18(11), 1004-1015, 2017.
- [29] Istanbul Metropolitan Municipality European Side Road Maintenance and Repair Directorate, Concrete Finishing with Concrete Paving on Roads Across Istanbul and Busway Stops on the BRT Route (Tender Code: 401962), *Special Technical Specifications For Concrete Paving Of Metrobus Road With Slipform Concrete Finisher*, 2021.

- [30] Akbulut, K., Bezgin, N.Ö., Kici, A., Discussion of the safety, serviceability and suitability of bus rapid transit services. In *Proceedings of the Institution of Civil Engineers-Transport* 175, 5, 251-260, 2022.
- [31] Turkish Radio and Television Corporation (TRT) Database, Database of the TRT Haber Database, Istanbul Türkiye. See <https://www.trthaber.com/haber/turkiye/metrobus-yollarinda-asfalt-eridi-calisma-120-gun-surecek-780106.html> (accessed 09/11/2024), 2024.
- [32] Mercedes, The technical specifications of the Conecto G model, *Germany*, 2019.
- [33] Mercedes, The technical specifications of the Capacity model, *Germany*, 2019.
- [34] Otokar, The technical specifications of the Otokar Kent XL model, *Türkiye*, 2022.
- [35] Ulasim AS., The technical specifications of the Akia Ultra LF 12 model, *Türkiye*, 2023.
- [36] Liu, B., Zhou, Y., Gu, L., Huang, X., Finite element simulation and multi-factor stress prediction model for cement concrete pavement considering void under slab. *Materials*, 13(22), 5294, 2020.
- [37] Sachs, S.G., Vandenbossche, J.M., Tompkins, D., Khazanovich, L., Establishing the interlayer structural response for unbonded concrete overlays of existing concrete pavements. *Transportation Research Record*, 2672(40), 254-263, 2018.
- [38] Davids, W.G., Turkiyyah, G.M., Mahoney, J.P., EverFE: Rigid pavement three-dimensional finite element analysis tool. *Transportation Research Record*, 1629(1), 41-49, 1998.
- [39] Bejarano, M.O., CRCP Design for guided bus route in the UK. *Airfield and Highway Pavements*, 477-487, 2015.
- [40] Higuera-Sandoval, C.H., Hernández-Rojas, D.A., Application of Finite Elements for the Check of Hydraulic Concrete Slabs. *Respuestas*, 26(2), 14-26, 2021.
- [41] Shaban, A.M., Alsabbagh, A., Wtaife, S., Suksawang, N., Effect of pavement foundation materials on rigid pavement response, *IOP Conference Series: Materials Science and Engineering*, 2020.
- [42] Cheng, G., Zheng, Y., Yu, J., Liu, J., Hu, X., Investigation of the Fatigue Life of Bottom-Up Cracking in Asphalt Concrete Pavements. *Applied Sciences*, 12(23), 12119, 2022.
- [43] Maitra, S.R., Reddy, K.S., Ramachandra, L.S., Numerical investigation of fatigue characteristics of concrete pavement. *International Journal of Fracture*, 189, 181-193, 2014.

## Finite Element Analysis of Concrete Gravity Dam

Tuba Aydin

Suleyman Demirel University, Faculty of Engineering and Natural Sciences, Department of Civil Engineering,  
Isparta, Turkey

✉: [tubaaydin@sdu.edu.tr](mailto:tubaaydin@sdu.edu.tr)  ID: 0000-0002-7404-5020

Received: 26.09.2024, Revised: 6.11.2024, Accepted: 20.11.2024

### Abstract

*Dams have been structures that have served to meet humanity's water needs for centuries. Because they are large structures, critical investigations must be made before they are built. However, these investigations and scaled or one-to-one modeling of dams have become costly today. At this point, package programs working with finite elements are used functionally. ANSYS package program is also a frequently preferred package program that provides results close to reality. In this study, a 3D dam body modeled with ANSYS was examined. While modeling, the water load acting outside the dam's own weight and the material properties of the dam body were taken into account and analyzed. The dam was modeled in accordance with its exact dimensions without any scaling. This study examines the stress and displacement of a concrete gravity dam under half-filled and fully filled conditions, highlighting significant differences in structural behavior. It was determined that the displacement and stress values found for the full state were higher than the half-full state.*

**Keywords:** ANSYS, Concrete Gravity Dam, Finite Element Analysis

### 1. Introduction

Dams are structures that create reservoirs by blocking a river valley, allowing for water storage. In addition to storing water, they have fundamental benefits such as raising the water level and creating a large water surface [1]. It is very important to build dams in order to raise the water level and meet the water and irrigation water needs in the region where the river is located. In Turkey, the flow regimes of rivers are irregular, so it is necessary to store water during periods of abundance. In dry seasons, the stored water is used. For this purpose, many dams have been constructed [2]. To serve various purposes, dams and water-raising structures have been constructed since ancient times in human history. Since water is of great importance for human survival, it is important to build dams that meet the specific needs of the region.

Since dams are large and costly water structures, it is important to conduct experimental or numerical analysis before their construction to anticipate potential problems and predict the behavior of these structures. In recent years, this has been made possible through various software programs. Experimental studies for water structures can be costly, which is another reason why software programs are preferred. Additionally, these software programs use finite element methods and provide users with the ability to model the water structure in detail, allowing for realistic results. ANSYS is a software package that uses finite element methods and includes many modules. It is frequently used in solving engineering problems and is also effectively utilized in the field of civil engineering.

Ahemad et al. modeled a gravity dam in 3D using the ANSYS 2020 software package. They conducted analysis for both the filled and empty states of the dam. Stress and pressure values under the effect of water load were determined. Analysis were performed for different loading combinations, and it was concluded that the dam was safe [3].

Saxena and Patel examined the dynamic characteristics of the Shahpurkandi Dam, a concrete gravity dam with a height of 55.5 meters, using the ANSYS finite element software package. They analyzed the modal response of the dam by considering the condition when the reservoir is fully filled. The model was created taking into account the dam-foundation interaction. It was also found that the fully filled reservoir condition is more critical compared to the empty reservoir condition. It was demonstrated that ANSYS is a reliable and suitable software for investigating the dynamic behavior of a structure [4].

Sharma and Nallasivam computed the static response of a 2D model of the Bhakra concrete dam using the finite element software ANSYS. To investigate the dam-foundation interaction, the dam was modeled in two different ways: one including both the dam and foundation, and the other considering only the dam structure. It was found that the highest displacement value in the dam occurred at the crest [5].

Todorov et al., investigated the behavior of an old gravity concrete dam in Bulgaria under different load conditions. Various water loads in the reservoir, dependent on the seasonal variations in water quantity, were applied to the structure. The analysis conducted with ANSYS revealed that the reservoir was appropriately designed according to the dam's load-carrying capacity [6].

Vipparthy performed a finite element analysis of the Indirasagar Polavaram gravity dam by keeping the upstream hydrostatic pressure constant and varying the downstream tailwater pressure. The concrete gravity dam was modeled in 2D. The analysis investigated displacement and stress values, and it was observed that the maximum stress values accumulated at the heel of the dam. It was concluded that the developed finite element model accurately predicted the linear and modal responses of the dam [7].

Silveira et al., conducted a finite element analysis using a typical Brazilian dam profile and seismic data from a Brazilian earthquake. The aim was to investigate the impact of foundation-reservoir interaction on the dynamic behavior of concrete gravity dams, focusing on natural frequencies and vibration modes for free vibration analysis. The dam model was created using the APDL part of the ANSYS software. Stress and displacement parameters for the dam were determined. It was suggested that, in the dynamic analysis of dams, all relevant parameters should be analyzed consistently with the existing conditions in the dam-reservoir-foundation system [8].

Messaad et al., investigated the dynamic behavior of the dam-reservoir-foundation system under seismic loading using the ANSYS software. The Oued Fodda concrete dam, located in Chlef in northwestern Algeria, was selected as a case study. Variations in the foundation stiffness can lead to changes in the stress and displacement values of the dam. It was suggested that considering the dam-foundation interaction would be beneficial for obtaining more reliable results [9].

Gao et al., investigated the phenomenon of stress concentration occurring in gallery voids within concrete gravity dams. They attempted to create stress distribution maps around the gallery voids and the gallery design using the ANSYS software. It was observed that variations

in the shape and size of the galleries could lead to changes in the stress distributions of the dam [10].

Wei et al., studied a hydroelectric power plant dam. The concrete gravity dam in question was modeled using ANSYS, and stress and displacement values were investigated. The analysis for the reservoir being fully filled or at normal water levels showed that the stress and displacement parameters of the gravity dam can vary [11].

Habib et al., summarized and compared the general findings of recent studies on the structural performance of roller-compacted concrete (RCC) dams. It was found that commercial software packages using the finite element method can predict the behavior of RCC dams. The condition of cracks in RCC dams serves as an important indicator of damage formation [12].

Taylan and Aydın examined the behavior of the Darıderesi II Dam, located in Isparta, under the influence of three different earthquakes. The dam was modeled in detail, and the analysis results were obtained using ANSYS. Displacement and stress values were determined as a result of the analyses conducted for the Kocaeli, Düzce, and Dinar earthquakes. According to the analysis results, it was observed that these earthquakes would not cause any failure in the dam body [13].

In this study, a concrete gravity dam was modeled in 3D using the ANSYS software. The stress and displacement values were examined for both the half filled and fully filled conditions of the concrete gravity dam downstream, in addition to the dam's own weight. It was found that the displacement and stress values obtained for the half filled condition were lower compared to those for the fully filled condition.

In previous studies, the behavior of rock-fill dams under the effect of water load has been examined. However, in this study, the displacement and stress values of a concrete gravity dam were investigated.

This paper is divided into sections under the headings of Materials and Methods, Finite Element Method and ANSYS Software, and Numerical Analysis-Results. Under the Materials and Methods section, the working principle of the finite element method and the details of the modules used within the ANSYS software are described in detail. The Numerical Analysis-Results section provides visual representations of the stress and displacement results for the 3D dam model.

## **2. Materials and Methods**

### **2.1. Finite Element Method**

The finite element method has become a widely preferred technique in solving engineering problems thanks to the development of sophisticated software packages. Particularly in complex and large geometries, various analysis are conducted using the finite element method. Large geometries are divided into manageable smaller elements and modeled in either two or three dimensions. The behavior of the structure under various static and dynamic loads applied to these models is then studied.

Software packages that use the finite element method are preferred because they provide realistic results and produce outcomes in a shorter time compared to experimental studies. Additionally, creating scaled models of large and complex geometries and conducting various

analysis can be very costly. Therefore, software packages play a crucial role in solving engineering problems by saving time and reducing costs.

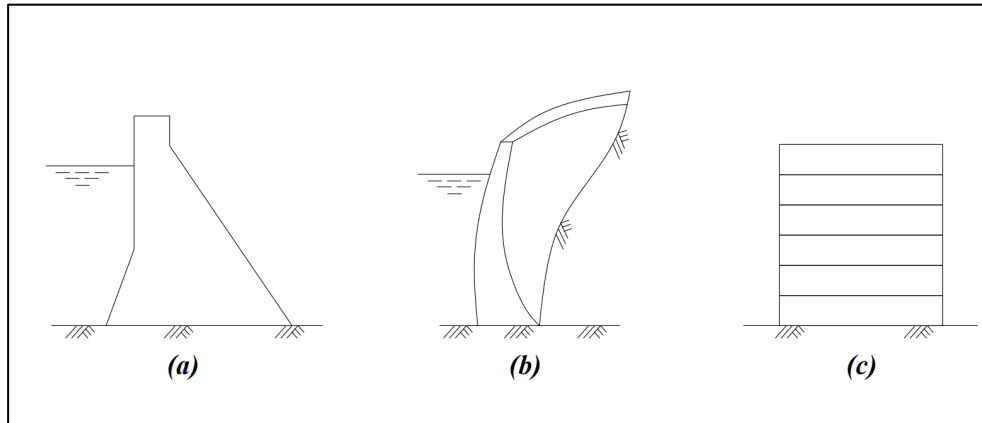


Fig. 1. Engineering structures

The behavior of various civil engineering structures, such as the concrete gravity dam body, arch dam body, and massive concrete blocks shown in Fig. 1, under different loads can only be analyzed using software packages. In Fig. 1. a, the concrete gravity dam body is nearly triangular in shape, although there is a slope in the upstream and downstream sections. Fig. 1. b shows an arch dam, which represents a dam body that continues in a parabolic shell shape. The material properties of the concrete gravity dam and the arch dam are also different from each other. Additionally, while the dam bodies are divided into meaningful geometries, both will be meshed with different elements. Fig. 1. c shows a massive concrete block used in the construction of a concrete gravity dam. Typically, a concrete layer 1.5-3.0 meters thick is poured every 6-10 days, leading to variations in the modulus of elasticity within each layer. Considering the influencing parameters within each structure and elasticity theory, it is not possible for theoretical methods to reflect realistic results. Given these considerations, numerical methods emerge as the sole solution for calculating stress values [14].

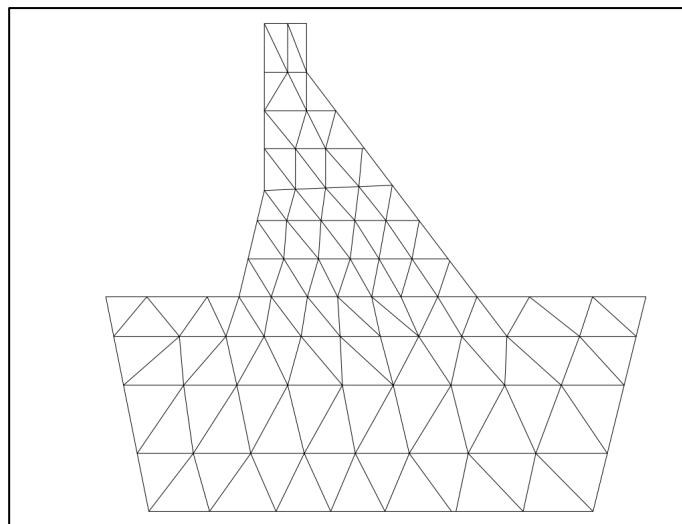


Fig. 2. Cross-section of the gravity dam divided into triangular elements

When using the finite element method, the structure to be analyzed is divided into finite elements. Fig. 2. shows the finite element representation of a concrete gravity dam body, divided into elements of a specific type. As seen in the figure, it consists of triangles of different



sizes. This way, the mesh structure conforms to the boundary conditions of the structure's shape. Additionally, it is worth noting that different types of elements can represent different material properties. The finite element method is employed to analyze complex structural problems in computer-based environments. Nowadays, this method is also preferred in construction, hydraulic, mechanical, and aerospace fields.

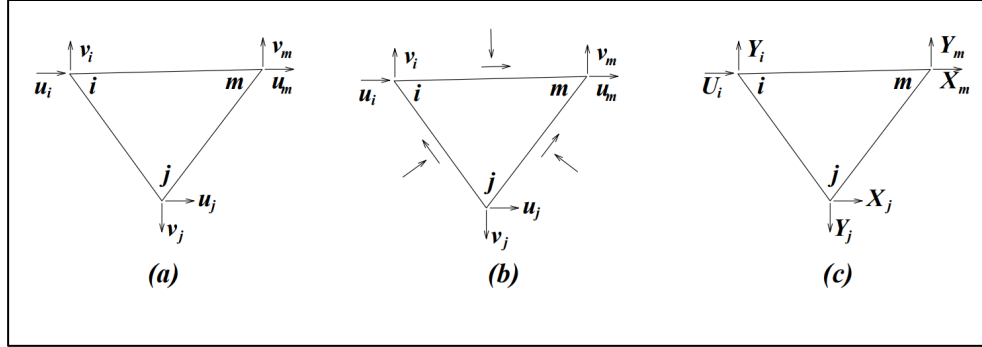


Fig. 3. Node displacements, equivalent node forces, and node loads of an element

The concrete gravity dam body in Fig. 2. is modeled as a 2-dimensional plate. The concrete gravity dam body can be divided into a specific number of triangular elements, as shown in Fig. 3. Each element has three nodes, and each node has two displacement components. Therefore, at each node of the element, there are a total of six displacement components [14].

The advantages of the finite element method include:

- It can be used for the analysis of structures with various shapes,
- Different material properties can be assigned to different elements used in the mesh structure,
- Due to the large number of unknowns, it is feasible to perform these computations on a computer [14].

The finite element method is a powerful numerical analysis technique that is widely preferred today. It is used not only for structural problems but also across many different engineering fields.

A simple model consisting of a dual-spring system is shown in the Fig. 4. The stiffness of the springs is defined as  $K_1$  and  $K_2$ , and the movement of the springs is restricted to the x-direction. The forces acting on nodes 1 and 2 are denoted as  $F_1$  and  $F_2$ , respectively. To determine the displacement parameter occurring in the springs;

$$F = K.X \quad (1)$$

**F**: Applied Force, **K**: Spring constant, **X**: Displacement

When an equation is formulated considering the parameters of the springs in the figure,

$$F_2 - (X_2 - X_1)K_2 = 0 \quad (2)$$

$$F_1 - XK_1 + (X_2 - X_1)K_2 = 0 \quad (3)$$

If this equation is written in matrix form, it will take the following form;

$$\begin{bmatrix} F_1 \\ F_2 \end{bmatrix} = \begin{bmatrix} K_1 & -K_2 & X_1 \\ -K_2 & K_2 & X_2 \end{bmatrix} \quad (4)$$

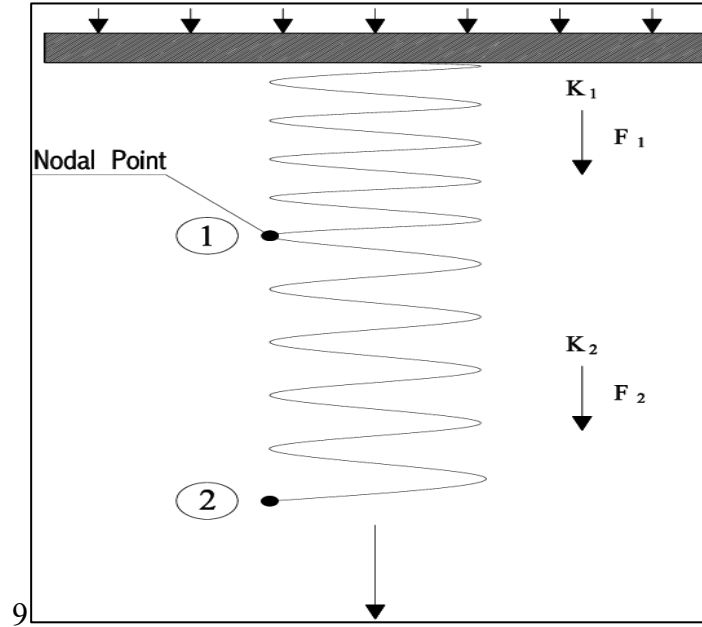


Fig. 4. Spring system

In this mathematical model, if the forces and spring constants are known, the displacement value occurring in the system can be calculated [15].

## 2. ANSYS Software

ANSYS is a package program frequently preferred in recent years for solving various engineering problems. It performs analysis using the finite element method and has two different modules: APDL and WORKBENCH. The APDL module assigns materials to models and analyzes their behavior under loads according to commands, while the WORKBENCH module performs analysis using visual commands on the screen without the need for command writing. The fundamental difference between the two modules, which operate on the same solution principle, is that the WORKBENCH module offers a more visual interface to the user. In this study, analysis were performed using the WORKBENCH module.

The Static Structural parameter within the WORKBENCH module was chosen for the analysis of the concrete gravity dam. The Static Structural parameter was modeled directly using the Space Claim drawing program available in the Geometry Fig. 5. shows the dimensions of the concrete gravity dam. As seen in the Fig. 5, the crest width of the concrete gravity dam is 7 meters, and the crest length is 257 meters. The concrete gravity dam model was created taking into account the crest length of 257 meters as shown in Fig. 4.

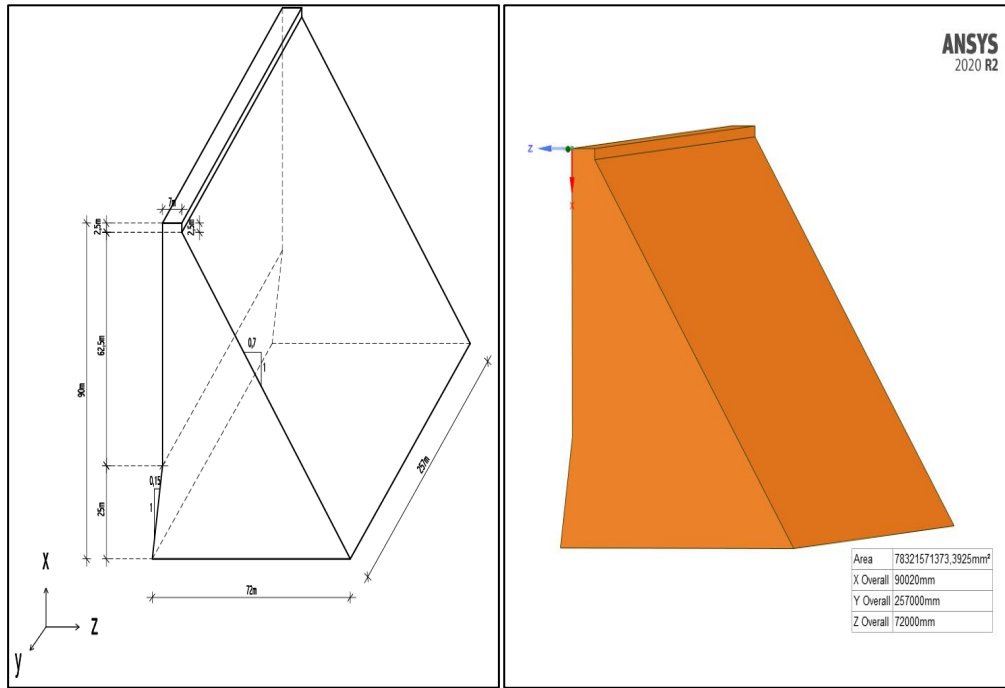


Fig. 5. Dimension of concrete gravity dam

Table 1. Material properties of concrete gravity dam

Material	Density $\gamma$ (kg/m <sup>3</sup> )	Young's Modulus E (Pa)	Poisson's Ratio $\nu$
Concrete	2300	3e+10	0,18

The behavior of the concrete gravity dam under water load effects was investigated. When defining the boundary conditions in the model, the material characteristics listed in Table 1. were specified first. After assigning the material, a mesh structure suitable for the dam's shape was applied. Then, since the dam is anchored to the slopes, a fixed support constraint was applied in these areas. Following the assignment of all boundary conditions, water load was defined for the model under both fully filled and half-filled condition. While examining the effect of water load, the effect of temperature was neglected and was not included in the boundary conditions.

Two different load cases were applied to the model equipped with the mesh structure: one for partially filled and one for fully filled conditions. Displacement and stress values were obtained for both the partially filled and fully filled conditions.

### 3. Numerical Analysis And Results

The stress and displacement values of the dam, modeled in three dimensions, were examined for the case of the reservoir being half full. Fig. 6. shows the water load for the half-filled condition of the dam. The water load is expected to create the highest stress at the base and the lowest stress at the dam surface. According to fluid mechanics principles, the stress due to the water load is represented in Fig. 6.

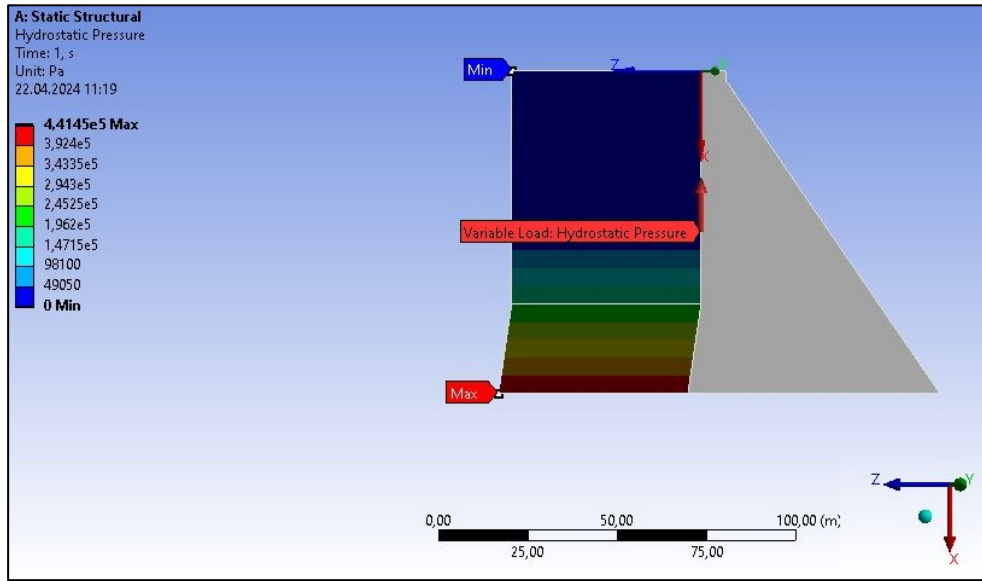


Fig. 6. Water load for the reservoir in the half-filled condition

For the half-filled condition of the dam, the stress and displacement values at the downstream section were examined. Fig. 7. shows the highest displacement value, which was found to be 0.00037326 meters. As expected, the highest displacement value is located in the middle part of the crest region.

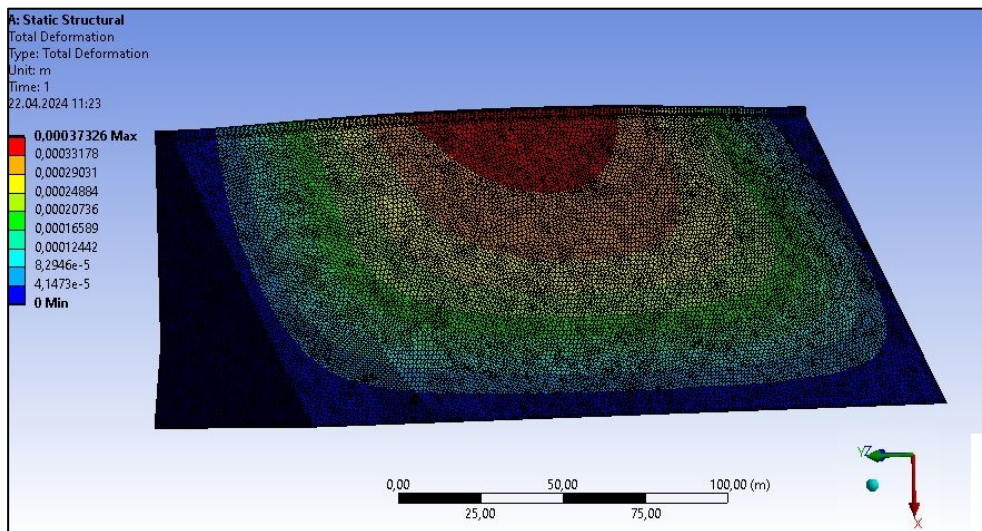


Fig. 7. Displacement at the downstream section of the dam in the half-filled condition

For the half-filled condition of the dam, a stress value was observed at the downstream section. As shown in Fig. 8, the highest stress value was found to be  $1.813 \times 10^6$  Pa. The lowest stress value observed was  $2.2585 \times 10^{-8}$  Pa.

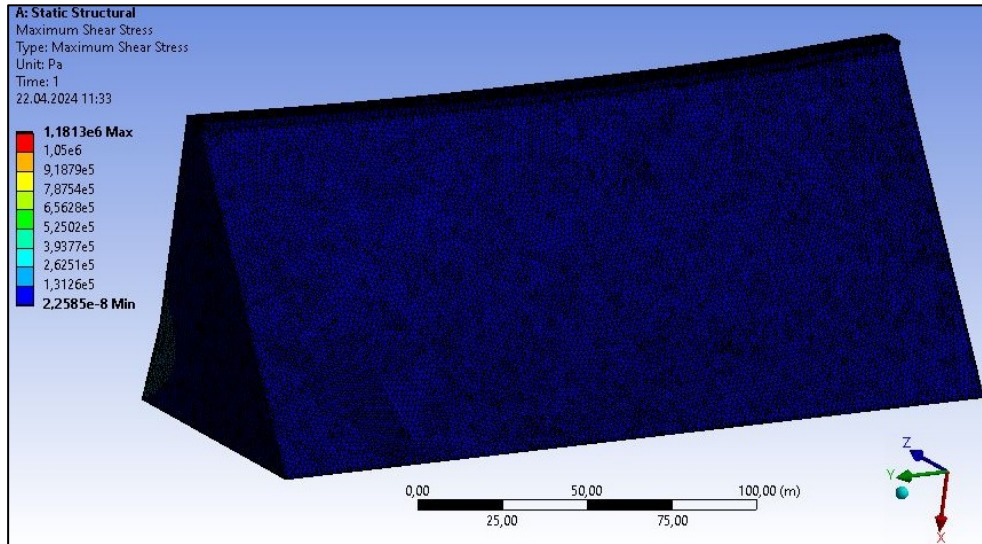


Fig. 8. Stress at the downstream section of the dam in the half-filled condition

Fig. 9. shows the water load for the dam in the fully filled condition. The water load is defined as lowest at the crest and highest at the base of the dam.

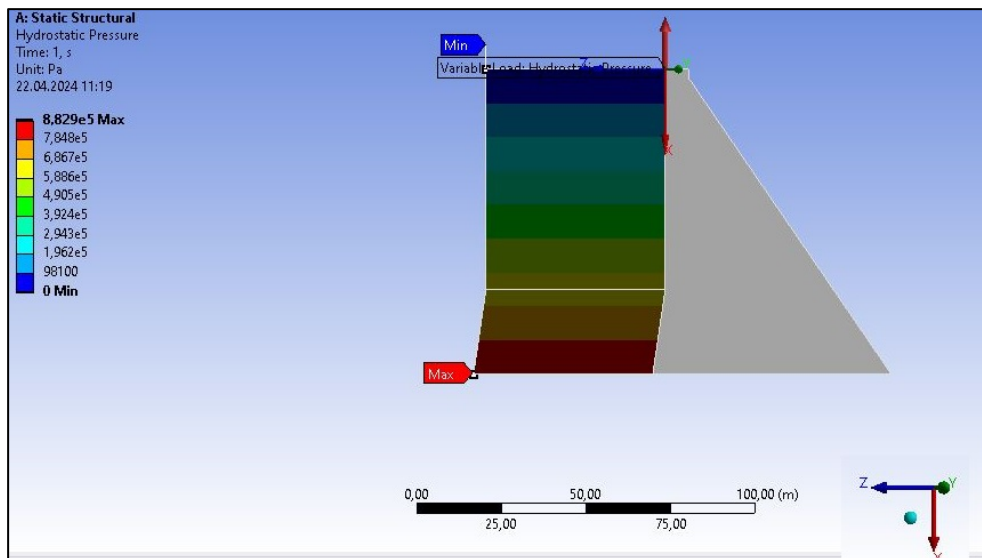


Fig. 9. Water load for the dam in the fully filled condition

Fig. 10. shows the displacement parameter at the downstream section of the dam in the fully filled condition. The displacement value was found to be 0.0075763 meters. As observed in the half-filled condition, the highest displacement value also occurs in the middle part of the crest region when the dam is fully filled.

For the case when the dam is completely full, a stress value has been generated at the downstream section. As shown in Fig. 11, the maximum stress value has been identified as  $3.5111 \times 10^6$  Pa. The minimum stress value is observed to be  $5.5282 \times 10^{-8}$  Pa.



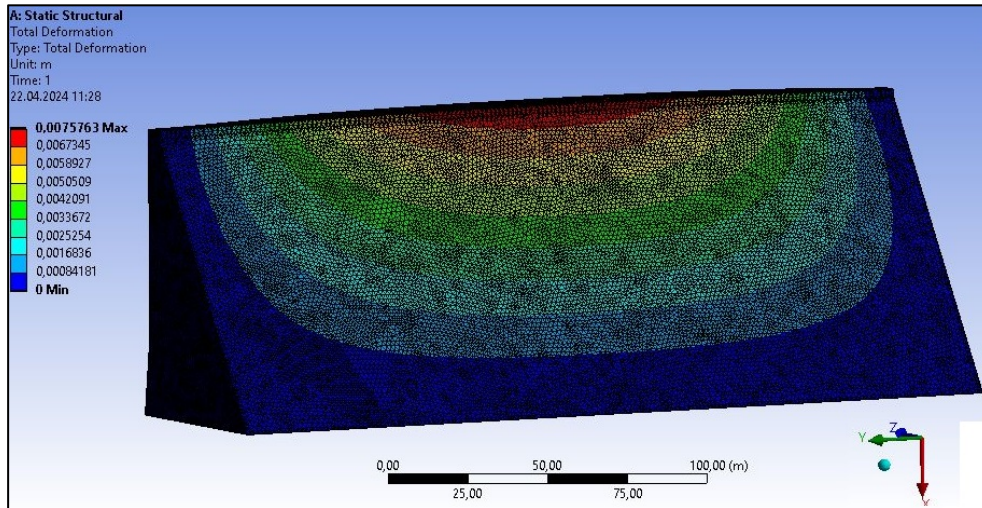


Fig. 10. Displacement at the downstream section of the dam in the fully filled condition

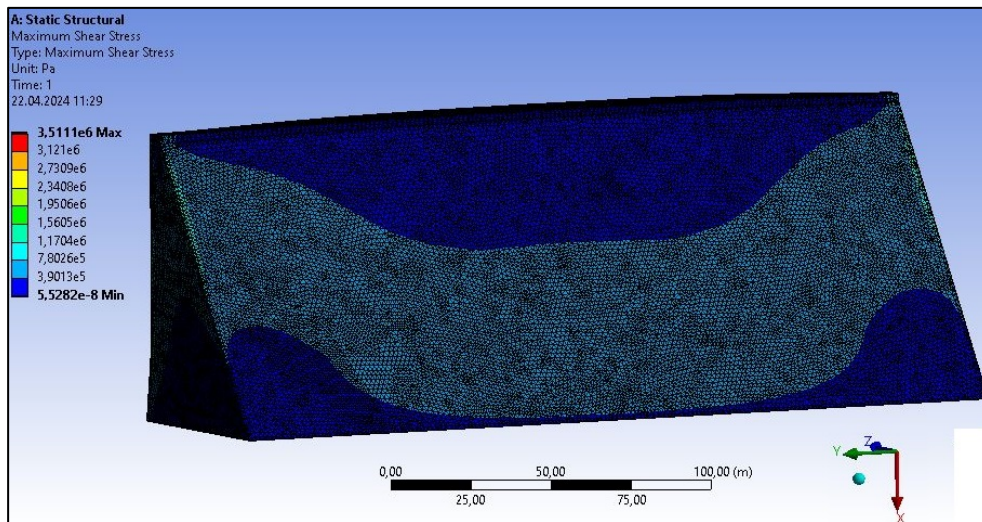


Fig. 11. Stress at the downstream section of the dam in the fully filled condition

#### 4. Conclusions

In this study, a concrete gravity dam has been examined, and the model of the dam was created in a 1:1 scale without any scaling. The lack of scaling is crucial for providing results that are close to reality regarding the stress and displacement values occurring in the dam. Analysis have been performed for the concrete gravity dam in both the half-filled and fully filled conditions. For these two cases, stress and displacement parameters have been determined and analyzed. During the analysis, attention was paid to equipping the structure with an appropriate mesh configuration, and the material properties were defined to be suitable for concrete gravity dams. Additionally, the water load was defined based on fluid mechanics principles and the height of the dam. The analyses were carried out with careful consideration of all these steps.

As a result of the analyses performed for the concrete gravity dam:

1. The displacement value obtained for the dam when fully filled is 0.0075763 m, whereas the displacement value when half-filled is 0.00037326 m. The larger displacement value in the fully filled condition is due to the effect of the water load.
2. The stress value obtained for the dam when fully filled is  $3.5111 \times 10^6$  PA, while for the half-filled condition it is  $1.813 \times 10^6$  PA. Similar to the displacement values, the higher stress value in the fully filled condition is the result of the water load effect.
3. In the study, the displacement and stress values at the downstream side of the concrete gravity dam were considered. The displacement and stress values at the upstream side of the dam will be examined in a subsequent study
4. The displacement value reaches its highest point in the middle of the crest area, as shown in the visuals. This is due to the fact that the concrete gravity dam is anchored to the slopes.
5. Large and costly structures such as concrete gravity dams can be modeled in detail using ANSYS, allowing critical parameters such as stress and displacement to be determined.
6. Unlike experimental studies conducted for dams, this approach is more cost-effective and provides results in a shorter amount of time.

## References

- [1] Ağırlioğlu, N., Baraj Planlama ve Tasarımı: cilt 1. Su Vakfı Yayınları, 2<sup>nd</sup> edition, 2007.
- [2] Erkek, C., Ağırlioğlu, N., Su Kaynakları Mühendisliği. Beta Basım Yayıncılık Distribution, 6<sup>th</sup> Ed., 2010.
- [3] Ahemad, F., Awar, U., Hanumanthappa, M. S., Stability analysis of gravity dam with is-code method and ANSYS. SAMRIDDHI: A Journal of Physical Sciences, Engineering and Technology, 14(3), 435-441, 2022.
- [4] Saxena, S., Patel, M., Evaluating dynamic behaviour of a concrete dam using modal analysis. Materials Today: Proceedings, 93, 296-301, 2023.
- [5] Sharma, A., & Nallasivam, K., Static analysis of a concrete gravity dam using the finite element technique. Asian Journal of Civil Engineering, 24(8), 2939-2957, 2023.
- [6] Todorov, O. K., Petkova, S. S., Kisliakov, D. S., Formulation of parameter limit values for the operation of a large concrete gravity dam, 12th International Scientific Conference Civil Engineering Design and Construction (DCB 2022), New York, USA, 7-10 September, 2022.
- [7] Vipparthy, R., Static and free vibration analysis of gravity dam under the influence of hydrostatic pressure using ANSYS finite element models, 2022. <https://doi.org/10.21203/rs.3.rs-1823407/v1>.



- [8] Silveira, I. V. D., Pedroso, L. J., Marotta, G. S., Study of the influence of the foundation and the reservoir on the dynamic response in a concrete gravity dam profile. *Revista IBRACON de Estruturas e Materiais*, 14(4), e14403, 2021. <https://doi.org/10.1590/S1983-41952021000400003>.
- [9] Messaad, M., Bourezane, M., Latrache, M., Berrabah, A. T., Ouzendja, D., Three-dimensional seismic analysis of concrete gravity dams considering foundation flexibility. *Mechanics and Mechanical Engineering*, 25(1), 88-98, 2021.
- [10] Gao, S., Chen, Y., Xiang, J., Finite element analysis of stress in the gallery of gravity dam on inclined bedrock based on ANSYS model. 2021 International Conference on Water Conservancy, Energy and Environmental Engineering, Nanjing, China, 25-27 June 2021.
- [11] Wei, L., Wei, P., & Yang, Y., Static calculation and analysis of certain gravity dam. In *Journal of Physics: Conference Series*, 1550 (3), 032006, IOP Publishing, 2020. doi:10.1088/1742-6596/1550/3/032006.
- [12] Habib, A., Hourri, A. A., Habib, M., Elzokra, A., Yildirim, U., Structural performance and Finite Element modeling of roller compacted concrete dams: A review. *Latin American Journal of Solids and Structures*, 18, e376, 2021.
- [13] Taylan, D., Aydın, T., Analysis of dynamic behavior of Darıderesi-II Dam by ANSYS. *Natural Hazards*, 90, 1223-1235, 2018.
- [14] Zhu, B., *The Finite Element Method: Fundamentals and Applications in Civil, Hydraulic, Mechanical and Aeronautical Engineering*, First Edition, 2018.
- [15] Ovalı, İ., *Ansys Workbench*. Kodlab Yayın Dağıtım Yazılım Ltd. Şti, 2018.